



**HAL**  
open science

## Synthetic silico-metallic particles-SSMMP-Ni and SSMMP-Ni-IL: CO<sub>2</sub> capture and utilization

Daniela Rodrigues, Julia Wolf, Barbara Polesso, Pierre Micoud, Christophe Le Roux, Franciele Bernard, François Martin, Sandra Einloft

► **To cite this version:**

Daniela Rodrigues, Julia Wolf, Barbara Polesso, Pierre Micoud, Christophe Le Roux, et al.. Synthetic silico-metallic particles-SSMMP-Ni and SSMMP-Ni-IL: CO<sub>2</sub> capture and utilization. Fuel, 2023, pp.128304. 10.1016/j.fuel.2023.128304 . hal-04285019

**HAL Id: hal-04285019**

**<https://hal.science/hal-04285019>**

Submitted on 14 Nov 2023

**HAL** is a multi-disciplinary open access archive for the deposit and dissemination of scientific research documents, whether they are published or not. The documents may come from teaching and research institutions in France or abroad, or from public or private research centers.

L'archive ouverte pluridisciplinaire **HAL**, est destinée au dépôt et à la diffusion de documents scientifiques de niveau recherche, publiés ou non, émanant des établissements d'enseignement et de recherche français ou étrangers, des laboratoires publics ou privés.



Distributed under a Creative Commons Attribution - NonCommercial - NoDerivatives 4.0 International License

# 1 Synthetic silico-metallic particles- SSMMP-Ni and SSMMP-Ni-IL: CO<sub>2</sub> capture and 2 utilization

3 Daniela Rodrigues<sup>1,3</sup>, Julia Wolf<sup>2</sup>, Barbara Polesso<sup>1</sup>, Pierre Micoud<sup>3</sup>, Christophe Le Roux<sup>3</sup>,  
4 Franciele Bernard<sup>2</sup>, François Martin<sup>3</sup>, Sandra Einloft<sup>1,2</sup>

5 <sup>1</sup>*Post-Graduation Program in Materials Engineering and Technology, Pontifical Catholic*  
6 *University of Rio Grande do Sul – PUCRS, Brazil.*

7 <sup>2</sup>*School of Technology, Pontifical Catholic University of Rio Grande do Sul PUCRS, Brazil.*

8 <sup>3</sup>*GET/OMP (CNRS, UT3PS, IRD, CNES), Université de Toulouse, ERT Géomatériaux,*  
9 *(Toulouse) France*

10

11 Abstract

12 Synthetic silico-metallic mineral particles (SSMMP) containing different amounts of Ni  
13 (SSMMP-Ni) and SSMMP-Ni functionalized with different IL (SSMMP-Ni-IL) were  
14 obtained and successfully used as solid adsorbents for CO<sub>2</sub> sorption, CO<sub>2</sub>/N<sub>2</sub>  
15 separation and highly recyclable heterogeneous catalysts active in the synthesis of  
16 different cyclic carbonates using CO<sub>2</sub> as a starting reagent. Samples were  
17 characterized by infrared spectroscopy (FTIR), RAMAN spectroscopy, X-ray diffraction  
18 (XRD), thermal analysis (TGA), specific surface area measurements (BET) and  
19 scanning electron microscopy (SEM). Samples containing IL demonstrated high CO<sub>2</sub>  
20 capture capacity (1.18-1.91 mmol CO<sub>2</sub>/g adsorbent - 1bar CO<sub>2</sub>), CO<sub>2</sub> selectivity (7.5-  
21 14.7) and stability. As catalysts, SSMMP-Ni 50% achieved a yield of 93.3% in  
22 propylene carbonate production (20 bar, 100°C and 7h) and constant yield up to 10  
23 cycles. These materials are easy to synthesize, with low energy demand, high stability  
24 and versatile to be used as adsorbent in CO<sub>2</sub> capture and catalyst for CO<sub>2</sub>  
25 transformation.

26

27 Keywords: CO<sub>2</sub>/N<sub>2</sub> separation; nickel synthetic silico-metallic mineral particles; CO<sub>2</sub>  
28 capture; CO<sub>2</sub> utilization; solid sorbents; heterogeneous catalysis

29

## 30 1. Introduction

31 The need to reduce the amount of CO<sub>2</sub> emitted into the atmosphere by the  
32 anthropogenic burning of fossil fuels is urgent. Energy production is majoritarian by  
33 fossil fuel and the prediction that it will continue in the next years is clear [1,2].  
34 Mitigating CO<sub>2</sub> emissions into the atmosphere is an imperative discussion to be

35 continued by heads of state and a huge challenge for scientists [3]. The portfolio of  
36 technologies available to reduce CO<sub>2</sub> concentrations in the atmosphere during this  
37 transition period of carbon-based to zero-carbon energy production includes CO<sub>2</sub>  
38 capture, utilization, and storage as mature options. Carbon capture and storage (CCS)  
39 aims to capture CO<sub>2</sub> before it is released into the atmosphere. After capturing the CO<sub>2</sub>,  
40 it is separated from the other gases and transported to geological storage. Among the  
41 available techniques, capturing CO<sub>2</sub> from gaseous effluents after fuel combustion is  
42 considered advantageous due to its integration into existing industrial facilities [2,4–7].  
43 Besides being the benchmark technology, chemical adsorption by aqueous solution  
44 amines presents some drawbacks, such as high volatility and low thermal stability, high  
45 cost of amine regeneration, degradation of amines and equipment corrosion [2]. Thus,  
46 the development of materials with high CO<sub>2</sub> capture efficiency and selectivity, low cost,  
47 and recyclability are urgent [8].

48 Problems related to CO<sub>2</sub> storage (such as the limited capacity for CO<sub>2</sub> geological  
49 storage, uncertainties regarding safety and storage time, and the lack of financial  
50 incentives), brought to light carbon capture and utilization technologies (CCU) [5,9].  
51 CCU presents the possibility of transforming residual CO<sub>2</sub> into a starting reagent in the  
52 production of industry-valuable chemical products. Cyclic carbonates can be used in  
53 industry as electrolytes in lithium batteries, monomers in polycarbonate synthesis,  
54 aprotic polar solvents, and reagents in the pharmaceutical industry and agricultural  
55 chemicals production [5,9,10]. However, CO<sub>2</sub> low reactivity and high thermodynamic  
56 stability demand the use of catalysts to the reaction efficiently occur with low energy  
57 expenditure. Homogeneous and heterogeneous catalysts are described for use in  
58 cyclic carbonates synthesis, including metallic salts [11], metallic oxides [12,13], ionic  
59 liquids [14], organic bases [15,16], metallic complexes [17,18] and metal-organic  
60 frameworks MOFs [19]. Homogeneous catalysts present good catalytic activity but the  
61 difficulty and cost of separating the product and catalyst are undesirable.  
62 Heterogeneous catalysts have drawbacks such as low catalytic activity, selectivity, and  
63 catalyst recyclability. Yet, the high energy demand for catalyst manufacture is an  
64 important issue [4,20]. In this scenario, it is imperative to continue the search for new  
65 efficient, recyclable, and low production cost heterogeneous catalysts.

66 The use of ionic liquids (IL) in CO<sub>2</sub> capture and transformation has been widely  
67 explored. In the first, as an alternative to amine solutions and in the second as  
68 homogeneous catalysts in carbonates synthesis. IL exhibits properties such as good

69 thermal stability, high ionic conductivity, good solubility, wide electrochemical potential  
70 window, high synthetic flexibility, non-flammable, recyclable and low vapor pressure  
71 and is classified as a green solvent [21–23]. However, the high viscosity of ILs results  
72 in low CO<sub>2</sub> diffusion and, consequently, low CO<sub>2</sub> sorption rates, making their use  
73 inconvenient for CO<sub>2</sub> capture [24]. An alternative to solve the inconvenience both as a  
74 homogeneous catalyst and for CO<sub>2</sub> absorption (high viscosity) is the use of IL  
75 supported on solid materials. Among the materials used as support are organic and  
76 inorganic polymers, silicas, nanoparticles, oxides, resins, MOFs and zeolites  
77 [2,7,10,24–31]. Silica-based materials are interesting to be used as support, they have  
78 many silanol groups (-SiOH) on their surface facilitating functionalization in addition to  
79 the affinity for the CO<sub>2</sub> [32]. SSMMP are synthetic talc precursor particles having a  
80 structure described as “nano-talc entities”. SSMMP are formed by 2-3 Mg octahedra  
81 with 3-4 Si tetrahedra distributed in the lower and upper part of the Mg octahedral  
82 “sheet”. After hydrothermal treatment, these “nano-talc entities” produce synthetic talc,  
83 stacked lamellae composed of octahedral sheets of Mg sandwiched by two tetrahedral  
84 sheets of Si bonded together by weak Van der Waals forces [33,34]. The main  
85 advantage of using SSMMP compared to synthetic talc is a large number of reactive  
86 groups (-SiOH and -MgOH) on the entire surface (against only 10% of the surface of  
87 synthetic talc), providing an excellent interaction with CO<sub>2</sub> and potentially synergistic  
88 effect with the IL [7,34,35]. Yet, the elimination of the step with the highest energy  
89 expenditure in the synthesis (hydrothermal treatment) makes these materials low-cost  
90 and easy to synthesize [7]. Partial and/or total Mg cation exchange by Ni and other  
91 divalent cations in the octahedral layer of synthetic talc was revisited and the  
92 application possibilities of these materials were also explored (Martin et al., 2019).  
93 The synthesis of SSMMP functionalized with IL, from a fast, one-step, low-energy  
94 method using only water as a solvent for dissolving the reagents places this material  
95 as a candidate for different applications [37]. SSMMP can be used as support materials  
96 for IL and further applied as solid materials for heterogeneous catalysis, heavy metal  
97 sorption and selective gas sorption [7]. Recently our group proved that Mg-based  
98 SSMMP can be used as a selective sorbent for CO<sub>2</sub>/N<sub>2</sub> separation [7].  
99 In this work, the synthesis and characterization of SSMMP with 50 and 100% of Ni  
100 replacing Mg were described. Yet, ammonium and imidazolium-based IL (20%) were  
101 supported by replacing Si during the synthesis. Obtained materials were further tested  
102 as solid adsorbents in CO<sub>2</sub> capture at 25°C, at CO<sub>2</sub> equilibrium pressures of 1-30 bar,

103 and as selective adsorbents for CO<sub>2</sub> in CO<sub>2</sub>/N<sub>2</sub> gas mixtures. Thinking in the possibility  
 104 of having CO<sub>2</sub> capture and transformation steps in the same place, SSMMP were also  
 105 tested as heterogeneous recyclable catalysts in the CO<sub>2</sub> cycloaddition reactions in  
 106 epoxides (10-30 bar, 60-110°C and 4-8 hours).

107

## 108 2. Experimental

109

### 110 2.1. Materials

111 Sodium metasilicate pentahydrate (Na<sub>2</sub>SiO<sub>3</sub>·5H<sub>2</sub>O, Sigma-Aldrich), sodium acetate  
 112 (CH<sub>3</sub>COONa, Sigma-Aldrich), magnesium acetate tetrahydrate ((CH<sub>3</sub>COO)<sub>2</sub>Mg·4H<sub>2</sub>O,  
 113 Sigma-Aldrich), acetic acid (CH<sub>3</sub>COOH, Sigma-Aldrich), nickel acetate tetrahydrate  
 114 (Ni(CH<sub>3</sub>COO)<sub>2</sub>·4H<sub>2</sub>O, Sigma-Aldrich), 1-triethoxysilylpropyl-n.n.n-methylimidazolium  
 115 chloride [IMI-Cl-silane], 1-trimethoxysilylpropyl-n.n.n-trimethylammonium chloride  
 116 ([AMO-Cl-Silane], Gelest), sodium bromide (NaBr, Sigma-Aldrich), sodium iodide (NaI,  
 117 Sigma-Aldrich), propylene epoxide (Sigma-Aldrich), styrene epoxide (Sigma-Aldrich),  
 118 1,2-epoxybutane (Sigma-Aldrich), epichlorohydrin (Sigma-Aldrich),  
 119 tetrabutylammonium bromide (TBAB, Sigma-Aldrich) and CO<sub>2</sub> (Air Liquide, 99.998%).  
 120 All reagents were used as purchased without further purification.

121

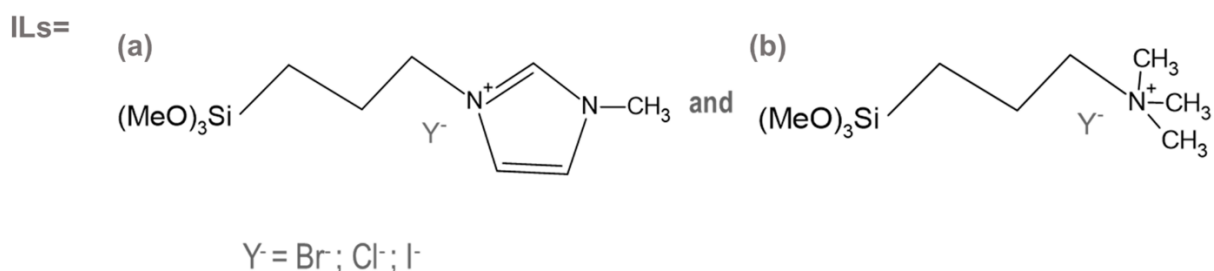
122 Table 1- Simplified scheme of samples synthesis reactions

Entry	Sample	Reaction equation
1	ST-Ni 50%	$4 [ \text{Na}_2\text{SiO}_3 ] + 1.5 [ \text{Ni}(\text{CH}_3\text{COO})_2 ] + 1.5 [ \text{Mg}(\text{CH}_3\text{COO})_2 ] + 2 \text{CH}_3\text{COOH} \rightarrow \text{ST-Ni } 50\% + 8 \text{CH}_3\text{COONa}$
2	SSMMP-Ni 50%	$4 [ \text{Na}_2\text{SiO}_3 ] + 1.5 [ \text{Ni}(\text{CH}_3\text{COO})_2 ] + 1.5 [ \text{Mg}(\text{CH}_3\text{COO})_2 ] + 2 \text{CH}_3\text{COOH} \rightarrow \text{SSMMP-Ni } 50\% + 8 \text{CH}_3\text{COONa}$
3	SSMMP-Ni 100%	$4 [ \text{Na}_2\text{SiO}_3 ] + 3 [ \text{Ni}(\text{CH}_3\text{COO})_2 ] + 2 \text{CH}_3\text{COOH} \rightarrow \text{SSMMP-Ni } 100\% + 8 \text{CH}_3\text{COONa}$
4	SSMMP-Ni 50%- IL*	$3.2 [ \text{Na}_2\text{SiO}_3 ] + 0.8 \text{IL-silane} + 1.5 [ \text{Ni}(\text{CH}_3\text{COO})_2 ] + 1.5 [ \text{Mg}(\text{CH}_3\text{COO})_2 ] + 2 \text{CH}_3\text{COOH} \rightarrow \text{SSMMP-Ni } 50\% - \text{IL} + 8 \text{CH}_3\text{COONa}$

123

\*IL = AMO-Br, AMO-Cl, AMO-I, IMI-Br, IMI-Cl and IMI-I

124



125

126 Figure 1- Structure of the ionic liquids functionalizing the SSMMP-Ni 50%. (a) [IMI-Y-

127

128

## 2.2. Synthetic talc synthesis

129 Synthetic talc with 50% Mg substituted by Ni (ST-Ni 50%) was synthesized using a

130 protocol well described in the literature [33,38]. Talc synthesis was carried out in two

131 stages: the first with the mixture of two solutions, a Si precursor, prepared from 0.2 mol

132 of Na<sub>2</sub>SiO<sub>3</sub>·5H<sub>2</sub>O dissolved in 200 mL of purified water, and another precursor solution

133 of Mg and Ni, prepared from 0.075 mol of Mg(CH<sub>3</sub>COO)<sub>2</sub>·4H<sub>2</sub>O, 0.075 mol of

134 Ni(CH<sub>3</sub>COO)<sub>2</sub>·4H<sub>2</sub>O and 0.1 mol of CH<sub>3</sub>COOH dissolved in 300 mL of purified water.

135 The second stage consists of the hydrothermal treatment of this mixture in an

136 autoclave for 6 hours, at 300°C, reaching a pressure of 85 bar. The talc gel obtained

137 after hydrothermal treatment is washed and centrifuged to remove the sodium acetate,

138 and dried in an oven at 100°C. The equation and the synthesis process of ST-Ni-50%

139 are represented in Table 1 (entry 1) and Figure 2.



140

141

Figure 2- Schematic representation of the synthesis of ST-Ni 50%

142

### 143 **2.3. Synthesis of SSMMP and SSMMP-IL**

144 Synthetic silico-metallic mineral particles (SSMMP) synthesis was recently described  
145 by our group [7]. The SSMMP containing Ni in substitution of 50% or 100% of the  
146 octahedral Mg (SSMMP-Ni 50% and SSMMP-Ni 100%, respectively) were synthesized  
147 in a similar way to the first step of the synthesis of ST-Ni 50% (described in the previous  
148 topic 2.2, without supplementary addition of CH<sub>3</sub>COONa in the Si precursor solution),  
149 with the exception for the synthesis of SSMMP-Ni 100% for which Mg(CH<sub>3</sub>COO)<sub>2</sub> is  
150 replaced by Ni(CH<sub>3</sub>COO)<sub>2</sub>. After mixing the precursor solutions of Si, Mg and Ni, the  
151 formed precipitate was washed with water and centrifuged until the complete removal  
152 of sodium acetate. Finally, the SSMMP-Ni X% were oven dried for approximately 24  
153 hours at 100°C. The formation reactions of SSMMP-Ni 50% and SSMMP-Ni 100% are  
154 shown in Table 1 (entries 2 and 3).

155 The synthesis of the SSMMP-Ni 50%-IL was performed by adapting the synthesis  
156 method described by Dumas (2013a). The ILs [IMI-Cl-Silane] and [AMO-Cl-Silane]  
157 were diluted in purified water and the Cl<sup>-</sup> anion was exchanged for Br<sup>-</sup> and I<sup>-</sup> anions  
158 using NaBr and NaI, respectively, resulting in ILs (IMI-Br, IMI-I, AMO-Br and AMO-I)  
159 as shown in Figure 1. The obtained ILs were mixed with the first solution of  
160 Na<sub>2</sub>SiO<sub>3</sub>·5H<sub>2</sub>O from formation synthesis of the SSMMP-Ni 50% following the same  
161 steps previously described for the synthesis of the SSMMP-Ni 50%, forming the  
162 samples named: SSMMP-Ni 50%-IMI Br, SSMMP-Ni 50%-IMI I, SSMMP-Ni 50%-AMO  
163 Br and SSMMP-Ni 50%-AMO I. The formation reaction of the SSMMP-Ni 50%-IL is  
164 represented in Table 1 (entry 4). In a typical SSMMP-Ni50% IL synthesis, the anion  
165 exchange was first performed using 0.08 mol of ILs (IMI-Cl-Silane or AMO-Cl-Silane)  
166 and 0.08 mol of the elected salt (NaBr or NaI) diluted in 100 mL of purified water, under  
167 constant stirring for 1 hour at room temperature. After the anion exchange, the IL-  
168 containing solution is mixed with a Si precursor solution (0.32 mol of Na<sub>2</sub>SiO<sub>3</sub>·5H<sub>2</sub>O  
169 dissolved in 300 ml of purified water). Finally, the solution containing the Si precursor  
170 and the IL is poured over the precursor solution of Mg and Ni (0.15 mol of  
171 Mg(CH<sub>3</sub>COO)<sub>2</sub>·4H<sub>2</sub>O and 0.15 mol of Ni(CH<sub>3</sub>COO)<sub>2</sub>·4H<sub>2</sub>O dissolved in 400 ml of  
172 purified water). The resulting precipitate is then centrifuged, washed with water and  
173 dried in an oven at 100°C.

174

175        **2.4. Materials characterization**

176 Perkin-Elmer FT-IR Spectrum 100 spectrometer in the range of 4000 cm<sup>-1</sup> to 600 cm<sup>-1</sup>  
177 was used to perform Fourier transform infrared spectroscopy (FT-IR). Confocal Raman  
178 microscopy system alpha300 R access from WiTec GmbH, equipped with a UHTS 300  
179 spectrophotometer with a diffraction grating of 600g/mm BLZ=500 nm and using a He-  
180 Ne laser was used to obtain RAMAN spectrograms. Thermogravimetric analyses  
181 (TGA) were obtained using a TA Instrument SDT-Q600. The temperature range was  
182 set at 25°C–900°C with a heating rate of 20°C/min, under nitrogen atmosphere. The  
183 specific surface areas were obtained using Brunauer-Emmett–Teller (BET) method.  
184 The nitrogen adsorption-desorption isotherm was obtained using NOVA 4200 High  
185 Speed at liquid nitrogen temperature. X-ray diffraction (XRD) analyses were performed  
186 on disoriented powders, using a Bruker D8 Advance diffractometer operating under  
187 the reflection of the CuK $\alpha_{1+2}$  radiation ( $\lambda = 1.5418 \text{ \AA}$ ), K $\alpha_2$  being subtracted with Bruker  
188 Diffrac. Eva software for figures. XRD patterns were collected over the 2-80°2 $\theta$  range,  
189 using 0.4 s counting time per 0.01°2 $\theta$  step at room temperature. The powdered talc  
190 skeletal density ( $\rho_s$ ) was measured at 25°C using an Ultrapycnometer 1000 -  
191 Quantachrome Corporation pycnometer using ultra-high purity helium (Air Liquide /  
192 99.999%). A field emission scanning electron microscope (FESEM) Inspect F50  
193 equipment (FEI Instruments) was used to assess particle morphology.

194        **2.5. CO<sub>2</sub> sorption capacity**

195 CO<sub>2</sub> sorption capacity was evaluated using well-described procedures [39,40]. The  
196 pressure decay technique reported by KOROS and PAUL was used to perform the  
197 tests Koros & Paul (1976), using an equilibrium cell equipped with two chambers (one  
198 being a gas chamber and the other a sorption chamber). Sorption tests were carried  
199 out in triplicates at a constant temperature of 25°C using CO<sub>2</sub> at equilibrium pressures  
200 of 1, 10, and 30 bar and sample mass of 0.6 to 0.7g. Before each test, the samples  
201 were placed in an oven remaining 1h at 100°C. Ten cycles of CO<sub>2</sub> sorption/desorption  
202 were performed to corroborate sample stability.

203        **2.6. CO<sub>2</sub> selectivity in CO<sub>2</sub>/N<sub>2</sub> mixtures**

204 CO<sub>2</sub> selectivity was performed with a mixture with a composition of 15:85 (v/v) of  
205 CO<sub>2</sub>/N<sub>2</sub> using the same CO<sub>2</sub> sorption system described above [42,43] CO<sub>2</sub> selectivity  
206 tests was performed at 20 bar of equilibrium pressure, and 25 °C of temperature, in



207 triplicate. For selectivity determination, two gas samples are taken from the system  
208 after the mixture pressure reaches equilibrium and injected into a gas chromatograph  
209 (GC) (Shimadzu GC-14B) equipped with a thermal conductivity detector to obtain the  
210 gaseous composition of the non-adsorbed mixture allowing the selectivity calculation  
211 as described in detail by Azimi and Mirzaei (2016).

212

$$213 \quad S = \frac{X_{CO_2}/Y_{CO_2}}{X_{N_2}/Y_{N_2}} \quad (1)$$

214

215 The selectivity CO<sub>2</sub>/N<sub>2</sub> is obtained using equation 1, where X<sub>CO<sub>2</sub></sub> and X<sub>N<sub>2</sub></sub>  
216 correspond to the molar fractions of CO<sub>2</sub> and N<sub>2</sub> sorbed by the sample, and Y<sub>CO<sub>2</sub></sub> and  
217 Y<sub>N<sub>2</sub></sub> are the molar fractions of CO<sub>2</sub> and N<sub>2</sub> present in the gas phase, respectively [7,42].

218

## 219 **2.7. Cyclic carbonates synthesis**

220 The synthesis of cyclic carbonates was carried out in a 120 mL titanium autoclave  
221 reactor. The system temperature is controlled by a thermocouple connected to a  
222 temperature controller. The reactor is charged with 0.1 mol of propylene oxide and 0.2  
223 g of catalyst. For the reactions carried out using a cocatalyst TBAB (0.6 mol% of EP)  
224 was added. The reactor was closed, pressurized with different CO<sub>2</sub> pressures (10-30  
225 bar) and heated (30-120 °C). The temperature was kept constant for a predetermined  
226 time (2-7 hours). After each reaction, the reactor was slowly cooled and depressurized.  
227 The catalyst was separated from the reaction product by centrifugation. The reaction  
228 product was treated under vacuum and heated to remove any remaining unreacted  
229 propylene oxide. The final product was analyzed using a Shimadzu GC-14B gas  
230 chromatograph, equipped with a flame ionization detector (FID) and an SH-Rtx-5  
231 column (30 m × 25 mm × 25 mm). A calibration curve with propylene carbonate as the  
232 internal standard and ethyl ether as solvent was previously constructed and used to  
233 determine reaction selectivity.

234 For cyclability tests, the catalyst was separated from the reaction product, washed with  
235 distilled water, centrifuged and dried in an oven at 100°C for approximately 2 hours.

236 After drying, the catalyst was ready to be reused in the next cycle, with the addition of  
237 cocatalyst TBAB (0.6 mol% of EP).

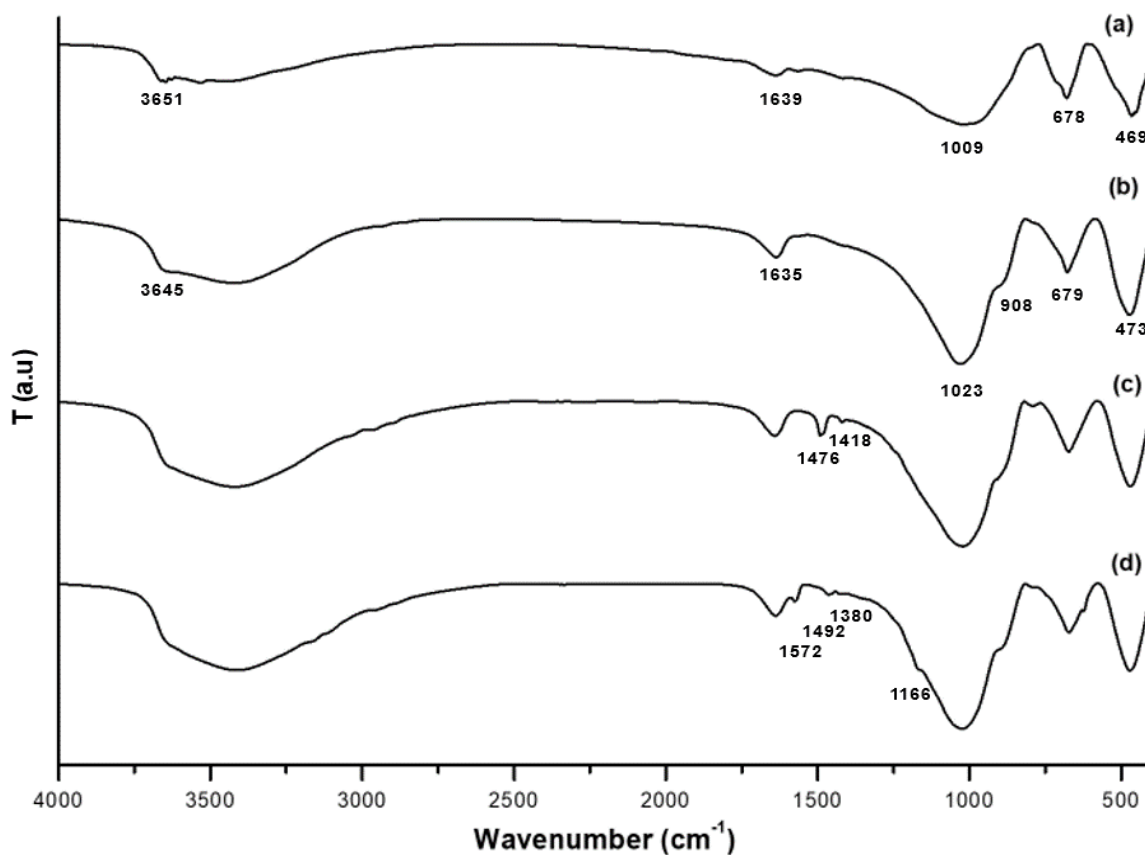
238

### 239 **3. Results and discussion**

#### 240 *FTIR*

241 ST-Ni 50%, SSMMP-Ni 50%, SSMMP-Ni 50%-AMO Br and SSMMP-Ni 50%-IMI Br  
242 FTIR spectra are presented in Figure 3, (a-d), respectively. For all samples,  
243 characteristic bands are seen at 3650  $\text{cm}^{-1}$  attributed to (-OH) stretching vibration of  
244 the  $\text{Mg}_3\text{-OH}$  and  $\text{Ni}_3\text{-OH}$ , at 1023  $\text{cm}^{-1}$  to symmetric stretching of Si-O-Si and Si-O, at  
245 678  $\text{cm}^{-1}$  to the overlapping of Ni-O and Si-O, and the OH groups deformation, and at  
246 473  $\text{cm}^{-1}$ , related to the stretching vibration of Si-O-Si and the -OH groups [44–51].  
247 The broad band at 3600-2800  $\text{cm}^{-1}$  is attributed to the water hydroxyl group (-OH)  
248 confirmed by the characteristic band at 1635  $\text{cm}^{-1}$  [52,53]. For SSMMP-Ni 50%-IMI Br  
249 (Figure 3, d), two characteristic bands are observed in the region of 1572  $\text{cm}^{-1}$  and  
250 1492  $\text{cm}^{-1}$ , related to the C=C stretch bond of the imidazolium ring present in the ILs  
251 cation. The bands located at 1380  $\text{cm}^{-1}$  and 1166  $\text{cm}^{-1}$  are attributed to C-H bonds of  
252 the IL aliphatic chain and the Si-C, respectively [54,55]. SSMMP-Ni 50%-AMO Br  
253 (Figure 3, c) evidenced the bands at 1476  $\text{cm}^{-1}$  and 1418  $\text{cm}^{-1}$  related to  $\text{CH}_2$  bond  
254 deformation [53,56]

255



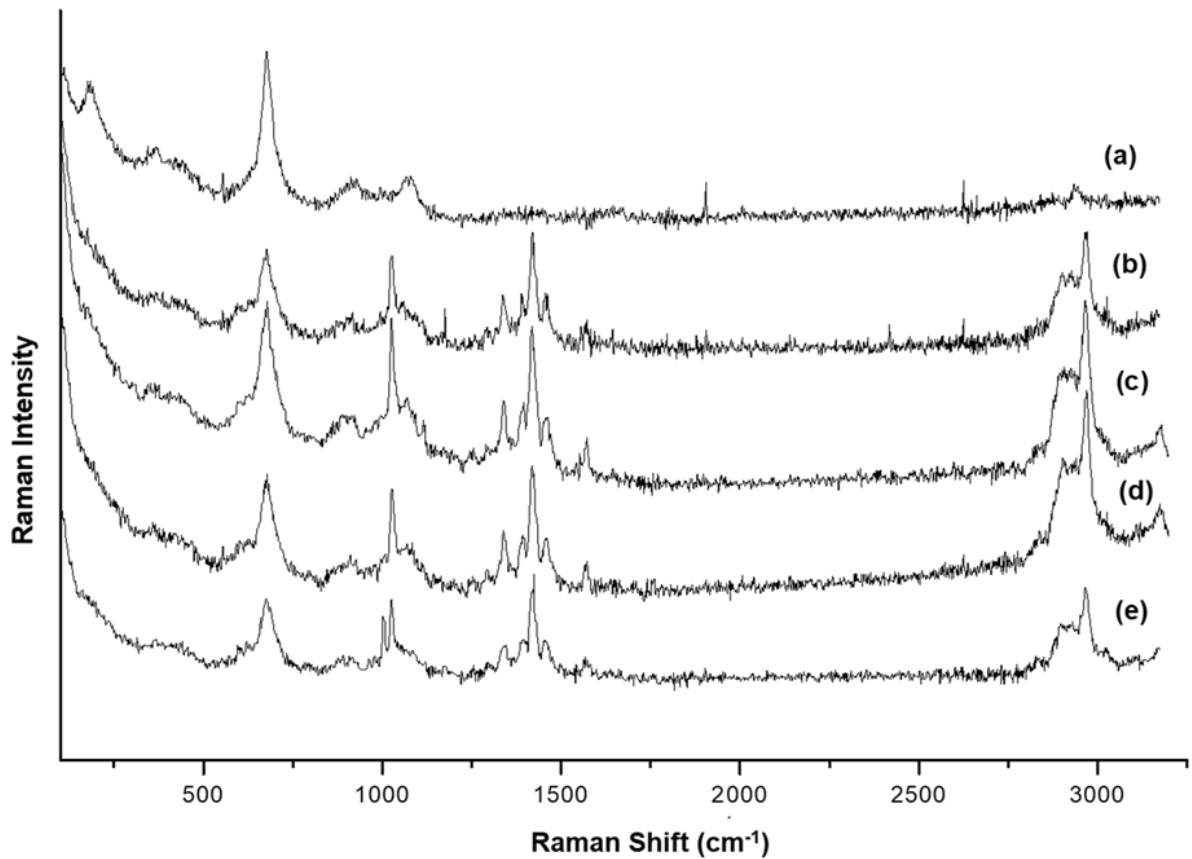
256

257 Figure 3- FTIR of samples (a) ST-Ni 50%, (b) SSMMP-Ni 50%, (c) SSMMP-Ni 50%-AMO Br  
 258 and (d) SSMMP-Ni 50%-IMI Br

259

260 *RAMAN*

261 Figure 4 presents Raman spectra of SSMMP-Ni 50% and SSMMP-Ni 50%-IL. For all  
 262 pristine and IL-functionalized samples a band near the 675  $\text{cm}^{-1}$ , attributed to the  
 263 symmetrical Si-O-Si elongation mode is observed [7,57]. For SSMMP-Ni 50%-IL  
 264 (Figure 4, b-e), new bands appeared in the region of 2902 and 2990  $\text{cm}^{-1}$ , characteristic  
 265 of the  $\text{CH}_2$ - and  $\text{CH}_3$ - bonds stretching vibrations present in the side chains of the  
 266 imidazolium and ammonium cations [7,58,59]. The bands between 900 and 1000  $\text{cm}^{-1}$   
 267 are attributed to C-C bonds stretching vibrations of the cation side chains. For  
 268 samples containing the ammonium cation (Figure 4, b and c), the bands at 1339  $\text{cm}^{-1}$ ,  
 269 1417  $\text{cm}^{-1}$  and 1560  $\text{cm}^{-1}$  are attributed to C-N,  $\text{CH}_2$ - and  $\text{CH}_3$ - bond asymmetric  
 270 stretching vibration, and  $\text{CH}_2$ -N bond vibration, respectively [59]. For samples  
 271 containing the imidazolium cation, bands in the same region (between 1326 and 1530  
 272  $\text{cm}^{-1}$ ) were observed and attributed to in the plane asymmetric stretching vibrations of  
 273 imidazolium ring (H-C-H, C-C,  $\text{CH}_2$ -N and  $\text{CH}_3$ -(N)-CN) [60].



274

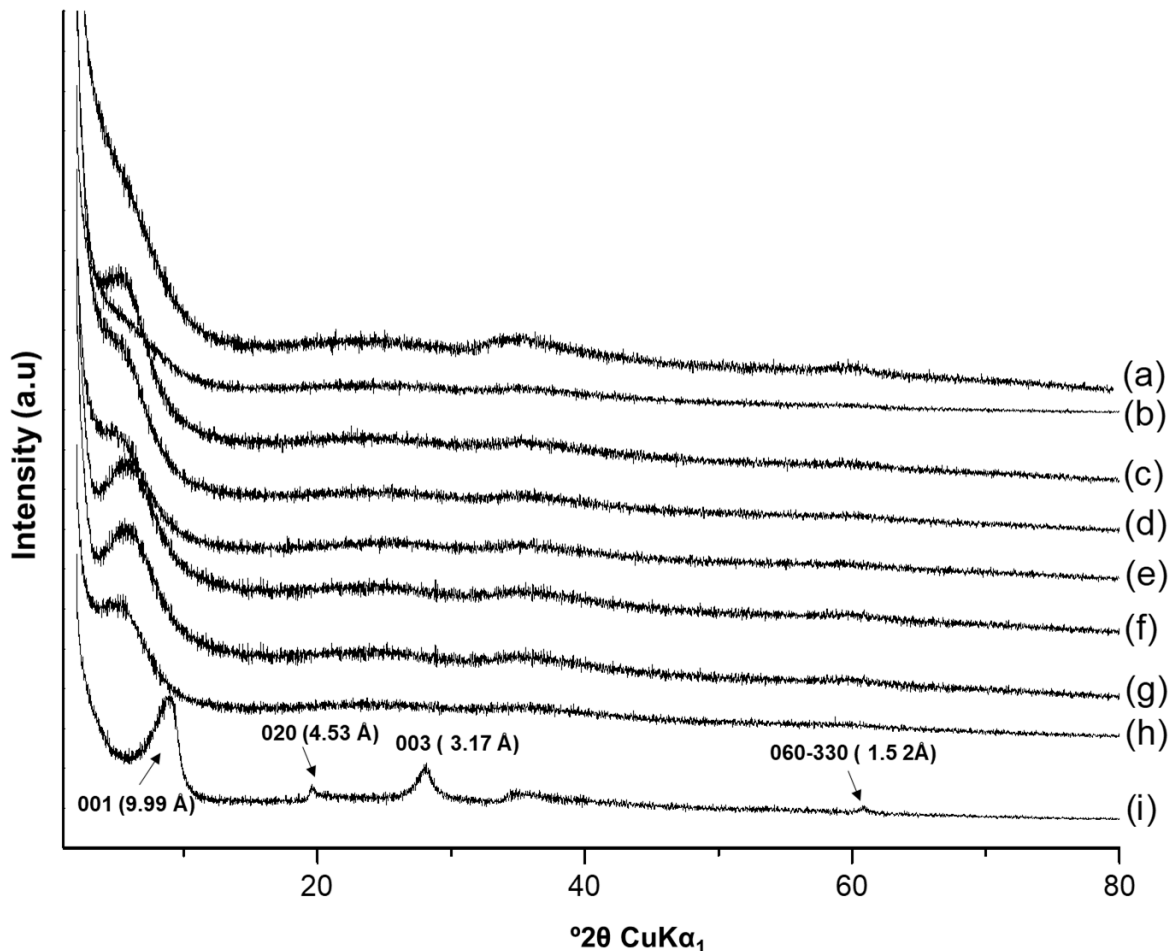
275 Figure 4- RAMAN spectra of samples (a) SSMMP-Ni 50%, (b) SSMMP-Ni 50%-AMO Br, (c)  
 276 SSMMP-Ni 50%-AMO I, (d) SSMMP-Ni 50%-IMI Br and (e) SSMMP-Ni 50%-IMI I

277

278 *XRD*

279 Samples XRD patterns are shown in Figure 5. ST-Ni 50% (Figure 5, h) presented inter-  
 280 reticular distance values (d) with reflections at 001 (9.99 Å), 020 (4.53 Å), 003 (3.17 Å)  
 281 and 060-330 (1.52 Å), characteristics of Mg/Ni synthetic talc [33,61]. SSMMP-Ni 50%  
 282 and SSMMP-Ni 100% (Figure 5, a and b) showed no reflection, evidencing the  
 283 formation of amorphous structures of SSMMP composed by two or three Mg and/or Ni  
 284 octahedrons and three or four Si tetrahedrons located at the top and the bottom of the  
 285 octahedral sheet; [33,34]. For samples functionalized with ILs (SSMMP-Ni 50%-IL,  
 286 Figure 5 c-g), a weak reflection at  $2\theta = 6^\circ$  is observed due to an increment in sample  
 287 structure organization caused by the surfactant effect of the organo-alkoxysilanes  
 288 present in the synthesis process acting as an anionic surfactant [62]. Yet, hydrophilic  
 289 groups form micelles facilitating Si-O-Mg covalent bond formation and assisting the  
 290 lamellar structure growth [34].

291



292

293 Figure 5- DRX patterns of samples (a) SSMMP-Ni 50%, (b) SSMMP-Ni 100%, (c) SSMMP-Ni  
 294 50%-AMO Cl (d) SSMMP-Ni 50%-IMI I, (e) SSMMP-Ni 50%-IMI Br, (f) SSMMP-Ni 50%-IMI  
 295 Cl, (g) SSMMP-Ni 50%-AMO I, (h) SSMMP-Ni 50%-AMO Br and (i) ST-Ni 50%.

296

### 297 TGA

298 Synthesized samples were characterized by TGA as seen in Table 2. Results show  
 299 that all samples have a first mass loss attributed to the loss of physisorbed water. The  
 300 second mass loss refers to the loss of Si-OH, Mg-OH and Ni-OH groups present on  
 301 the synthetic talc sheet edges (for ST-Ni 50%) or present in the surface of SSMMP  
 302 [7,63]. For samples functionalized with IL, the second step is also related to  
 303 imidazolium (starting near 280°C) and ammonium cations degradation (starting near  
 304 250°C) [53,64]. The third mass loss, appearing for synthetic talc ST-Ni 50%, refers to  
 305 the dehydroxylation of talc sheets accompanied by the formation of enstatite and silica  
 306 [51,63].

307

Table 2- Thermogravimetric analyses

Sample	1st mass loss		2nd mass loss		3rd mass loss	
	$T_{onset}$ - $T_{endset}$ (°C)	w/w %	$T_{onset}$ - $T_{endset}$ (°C)	w/w %	$T_{onset}$ - $T_{endset}$ (°C)	w/w %
ST-Ni 50%	25-137	4.4	137-550	2.9	550-900	3.0
SSMMP-Ni 50%	25-243	15.1	243-900	7.8	-	-
SSMMP-Ni 100%	25-258	16.2	325-900	7.4	-	-
SSMMP-Ni 50%-AMO Br	25-245	14.4	245-900	13.9	-	-
SSMMP-Ni 50%-AMO Cl	25-251	15.1	251-900	16.0	-	-
SSMMP-Ni 50%-AMO I	25-237	14.3	237-900	13.2	-	-
SSMMP-Ni 50%-IMI Br	25-293	10.8	293-900	13.2	-	-
SSMMP-Ni 50%-IMI Cl	25-283	13.5	283-900	18.0	-	-
SSMMP-Ni 50%-IMI I	25-279	11.9	279-900	12.0	-	-

309

310 *BET*

311 Table 3 presents the samples specific surface areas. SSMMP-Ni 50% and SSMMP-Ni  
312 100% present higher specific surface area when compared to ST-Ni 50% and SSMMP  
313 functionalized with IL (see Table 3, entries 2 and 3). SSMMP-Ni 50% was submitted to  
314 hydrothermal treatment to produce synthetic talc ST-Ni 50% decreasing the material  
315 specific surface area (from 285 m<sup>2</sup>/g to 195 m<sup>2</sup>/g). The drop in sample specific surface  
316 area after heat treatment results from the growth of SSMMP entities forming stacked  
317 lamellae with temperature [33,51]. The decrease in the specific surface area of the IL  
318 functionalized samples (see Table 3, entries 4 to 9) indicates the success of the IL  
319 insertion in the SSMMP structure [6,7]. Somehow the synthesis method of samples  
320 functionalized with IL interferes on the specific surface area value. Samples with Cl as  
321 anion undergo no anion exchange, while I and Br are inserted in the molecule by an  
322 ionic exchange reaction having NaCl as a byproduct. NaCl remains in the next step of  
323 the synthesis, probably facilitating defect creation during the washing process  
324 increasing specific surface area [65–67]. This idea can be corroborated by N<sub>2</sub>  
325 sorption/desorption curves showing a decrease in the N<sub>2</sub> volume adsorbed by the  
326 samples containing the Cl<sup>-</sup> anion (see Figure S1).

327

328

Table 3- Samples specific surface areas

Entry	Sample	S <sub>BET</sub> (m <sup>2</sup> /g)
1	ST-Ni 50%	145
2	SSMMP-Ni 50%	285
3	SSMMP-Ni 100%	340
4	SSMMP-Ni 50%-AMO Br	180

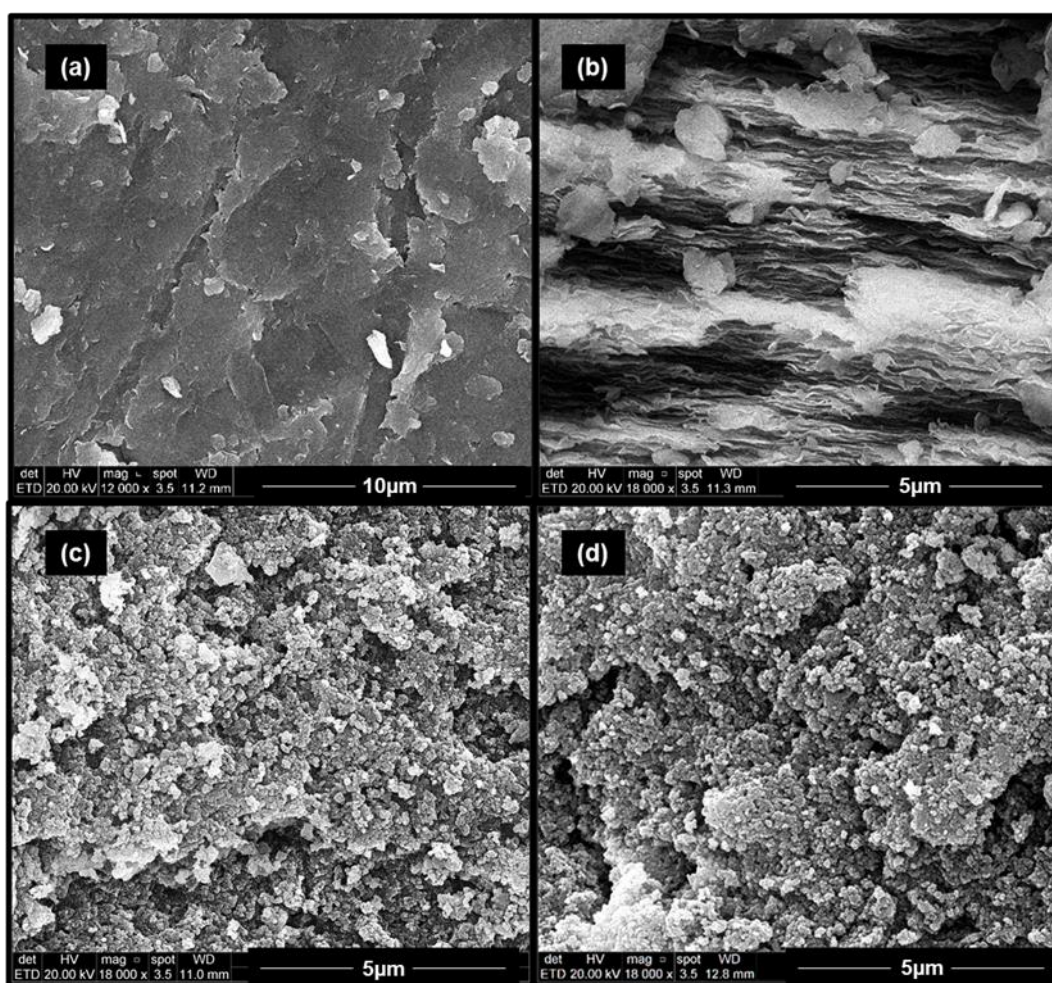
5	SSMMP-Ni 50%-AMO Cl	9.7
6	SSMMP-Ni 50%-AMO I	176
7	SSMMP-Ni 50%-IMI Br	211
8	SSMMP-Ni 50%-IMI Cl	27
9	SSMMP-Ni 50%-IMI I	213

329

330 SEM

331 Samples morphology is shown in Figure 6. ST-Ni 50% (Figure 6, a and b) has a dense  
 332 and compact structure, formed by numerous stacked lamellae. Samples undergoing  
 333 no heat treatment (SSMMP-Ni 50%, 100% and SSMMP-Ni 50%-IL) (Table 3, entries  
 334 2-9) showed agglomerated spherical morphology as seen in Figure 6 (c) and (d)  
 335 (samples SSMMP-Ni 50% and SSMMP-Ni 50%-AMO Br, respectively). CO<sub>2</sub> sorption  
 336 capacity is influenced by sample morphology. A particulate morphological structure  
 337 fosters CO<sub>2</sub> adsorption as seen in the next section.

338



339

340 Figure 6- Samples SEM images: (a) and (b) ST-Ni 50%, (c) SSMMP-Ni 50% and (d)  
 341 SSMMP-Ni 50%-AMO Br

342

343 **3.1 CO<sub>2</sub> sorption tests**

344 CO<sub>2</sub> sorption tests at CO<sub>2</sub> equilibrium pressures of 1 bar, 10 bar, and 30 bar of CO<sub>2</sub> at  
345 25°C are shown in Table 4. As expected, the synthetic talc ST-Ni 50% (Table 4, entry  
346 1) showed the lowest CO<sub>2</sub> sorption capacity among the analyzed samples. The low  
347 CO<sub>2</sub> sorption capacity presented by ST-Ni 50% is directly related to its lamellar  
348 structure composed of an octahedral sheet of Mg and Ni sandwiched by two tetrahedral  
349 sheets of Si presenting reactive groups (-SiOH and -MOH where M = Mg and Ni) only  
350 on the edges of these sheets (representing only 10% of the total surface) [34,35].  
351 According to previously published work [7], the OH groups are essential for the  
352 CO<sub>2</sub>/adsorbent interaction. The CO<sub>2</sub> sorption in adsorbents rich in Si-OH groups occurs  
353 by physical adsorption through dispersive and electrostatic interactions, by weak  
354 interaction of CO<sub>2</sub> with the OH group present on the surface of these materials  
355 ( $H^{\delta+} \dots \delta^- O=C=O^{\delta-}$ ) [7,68]. The above statement can be corroborated by comparing  
356 the CO<sub>2</sub> sorption capacity of synthetic talc ST-Ni 50%, and its precursor SSMMP-Ni  
357 50% (undergoing no thermal treatment) and SSMMP-Ni 100% (100% of the Mg  
358 replaced by Ni, undergoing no thermal treatment) (Table 4, entries 2 and 3,  
359 respectively). Comparing these two precursors with ST-Ni 50%, an increase of 0.61  
360 mmolCO<sub>2</sub>/g and 0.48 mmolCO<sub>2</sub>/g in the CO<sub>2</sub> sorption capacity, respectively, is  
361 observed at 1 bar. Unlike synthetic talc, SSMMP-Ni X% are formed by a few Si  
362 tetrahedra bonded together, sandwiching 1-3 octahedra of Mg/Ni (as shown in Figure  
363 7), this configuration allows the presence of greater amounts of reactive groups (-SiOH  
364 and -MOH where M= Mg and Ni) on the SSMMP surface and consequently higher  
365 interaction with the CO<sub>2</sub> [7,33,34,51].

366

367 Table 4 – Samples sorption capacity at 25°C in different CO<sub>2</sub> equilibrium pressures

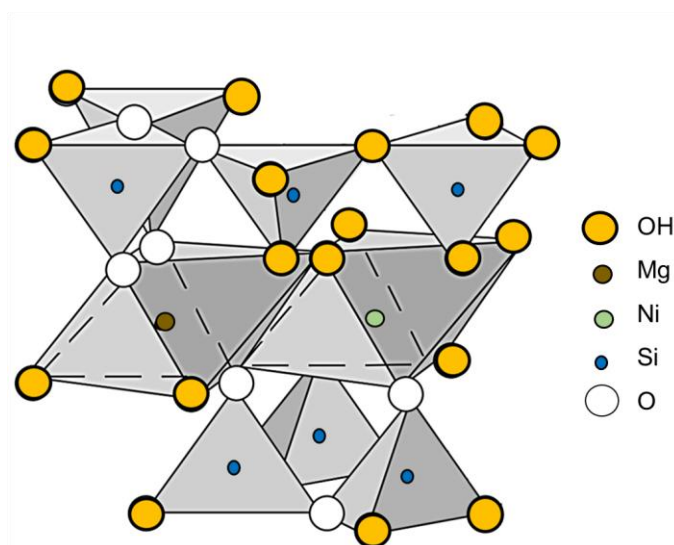
Entry	samples	CO <sub>2</sub> sorption		
		1 bar <sub>eq.</sub> (mmolCO <sub>2</sub> /g)	10 bar <sub>eq.</sub> (mmolCO <sub>2</sub> /g)	30 bar <sub>eq.</sub> (mmolCO <sub>2</sub> /g)
1	ST-Ni 50%	0.97 (±0.06)	2.42 (±0.09)	4.05 (±0.23)
2	SSMMP-Ni 50%	1.58 (±0.07)	3.26 (±0.18)	5.49 (±0.19)
3	SSMMP-Ni 100%	1.45 (±0.06)	4.21 (±0.20)	6.15 (±0.18)
4	SSMMP-Ni 50%-AMO Br	1.91 (±0.06)	3.84 (±0.16)	8.22 (±0.27)
5	SSMMP-Ni 50%-AMO Cl	1.25 (±0.06)	3.07 (±0.11)	4.63 (±0.06)



6	SSMMP-Ni 50%-AMO I	1.73 ( $\pm 0.07$ )	3.65 ( $\pm 0.04$ )	5.66 ( $\pm 0.13$ )
7	SSMMP-Ni 50%-IMI Br	1.64 ( $\pm 0.05$ )	3.42 ( $\pm 0.06$ )	7.92 ( $\pm 0.15$ )
8	SSMMP-Ni 50%-IMI Cl	1.18 ( $\pm 0.05$ )	2.87 ( $\pm 0.12$ )	4.45 ( $\pm 0.23$ )
9	SSMMP-Ni 50%-IMI I	1.61 ( $\pm 0.05$ )	3.73 ( $\pm 0.08$ )	4.98 ( $\pm 0.13$ )

368

369



370

371

Figure 7- SSMMP-Ni 50% structure

372 At low CO<sub>2</sub> equilibrium pressures, the SSMMP-Ni 50% functionalized with the ILs  
 373 AMO-Br, AMO-I, IMI-Br and IMI-I (Table 4, entries 4,6,7 and 9, respectively),  
 374 demonstrated slightly higher CO<sub>2</sub> sorption capacity when compared to pristine  
 375 SSMMP-Ni 50% (Table 4, entry 2). Even with the decrease in the specific surface area,  
 376 the SSMMP containing the ILs demonstrated a good CO<sub>2</sub> sorption capacity evidencing  
 377 the affinity CO<sub>2</sub>/IL. By analyzing the behavior of ammonium (AMO+) and imidazolium  
 378 (IMI+) cations in CO<sub>2</sub> capture, it can be seen that, regardless of the anion, SSMMP-  
 379 containing ammonium cation presented superior CO<sub>2</sub> sorption capacity. The same  
 380 behavior was observed by Tang et al., (2009) [69] when studying the CO<sub>2</sub> sorption  
 381 capacity in different poly (ionic liquids) containing ammonium and imidazolium cations.  
 382 This behavior was attributed to a stronger interaction between the ammonium cation  
 383 and CO<sub>2</sub> compared to the imidazolium cation and CO<sub>2</sub>. Ammonium cation possesses  
 384 a strong positive charge density compared to the delocalized positive charge of the  
 385 imidazolium cation facilitating CO<sub>2</sub>/IL interaction [70].

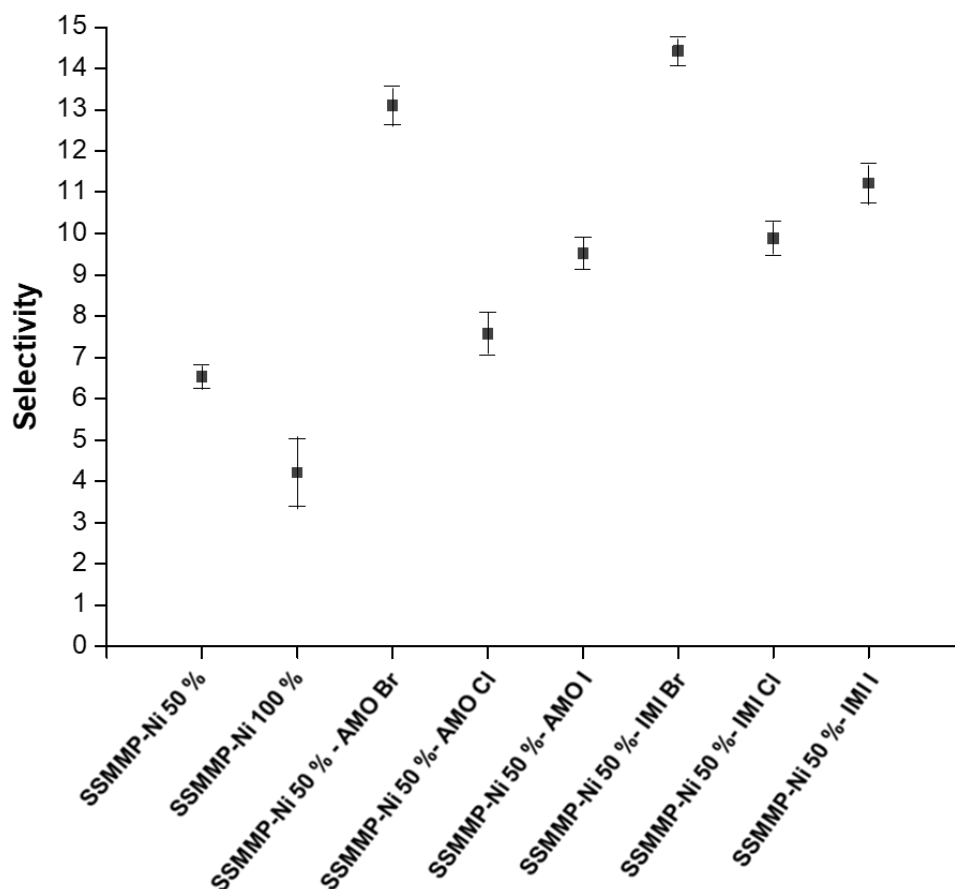
386 Furthermore, from the results shown in Table 4, it can be observed that the anion also  
387 plays an important role in CO<sub>2</sub> sorption. When comparing the anions Br<sup>-</sup> and I<sup>-</sup>, it is  
388 observed that regardless of the cation, the anion Br<sup>-</sup> has better CO<sub>2</sub> sorption capacity  
389 when compared to the anion I<sup>-</sup>. For halide anions, the interaction strength (binding  
390 energy) between anion-CO<sub>2</sub> decreases with increasing anion size, explaining the Br<sup>-</sup>  
391 superior sorption capacity [71]. Zhou et al.,(2016) [73] synthesized ZrP and MMT nano-  
392 sheets grafted with the IL BMIM Cl and analyzed their CO<sub>2</sub> sorption capacity. According  
393 to the author, at temperatures close to 40°C and at low CO<sub>2</sub> pressures, CO<sub>2</sub> sorption  
394 occurs by physical adsorption. Pristine SSPPM-Ni 50% and SSPPM-Ni 50% IL also  
395 adsorbs CO<sub>2</sub> by physisorption through the reactive groups (-SiOH and -MOH where M  
396 = Mg and Ni) of the SSMMP-Ni 50% surface and the ILs. In a recently published work  
397 by the group [7] two imidazolium-based ILs were functionalized onto Mg-based  
398 SSMMP varying the amount of silica substituted by grafted ILs from 5% to 20%. In  
399 conclusion, there is an ideal amount of IL to be functionalized on the SSMMP to  
400 maintain the synergistic relation between IL/reactive groups on the surface of the  
401 SSMMP.

402

### 403 **3.2 CO<sub>2</sub>/ N<sub>2</sub> selectivity tests**

404 Figure 8 presents CO<sub>2</sub> selectivity in CO<sub>2</sub>/N<sub>2</sub> mixtures for samples SSMMP-Ni X% and  
405 SSMMP-Ni 50%-IL. Comparing SSMMP-Ni X% with IL functionalized samples, it is  
406 clear that IL plays a role in CO<sub>2</sub> selectivity as previously related in literature  
407 [7,26,29,72,74]. The functionalization of SSMMP-Ni 50% with IMI-Br and AMO-Br  
408 increased CO<sub>2</sub> selectivity from 6.5 (±0.29) to 14.4 (±0.35) and 13.1 (±0.47), an increase  
409 of 121.5% and 101.5% in CO<sub>2</sub> selectivity, respectively. So the cation plays a role in  
410 CO<sub>2</sub> selectivity: SSMMP-Ni 50%-IMI samples are more selective for CO<sub>2</sub> when  
411 compared to SSMMP-Ni 50%-AMO with the same anion (see Figure 8). The anion also  
412 plays a role in CO<sub>2</sub> selectivity, Br<sup>-</sup> being the most selective above I<sup>-</sup> and Cl<sup>-</sup> (see Figure  
413 8).

414



415

416 Figure 8 – CO<sub>2</sub> selectivity in CO<sub>2</sub>/N<sub>2</sub> mixtures at 25°C and mixture equilibrium  
417 pressure of 20 bar.

418 Table 5 presents sorption capacity and CO<sub>2</sub> selective sorption for ionic liquids  
419 functionalized silica-based materials reported in the literature. As seen in Table 5, the  
420 SSMMP-Ni 50%-IL presented higher CO<sub>2</sub> sorption capacity at 1 bar when compared  
421 to the different sorbents represented in Table 5. Yet, when comparing the synthesis  
422 methods of most silica-based supports (Table 5) with SSMMP-Ni 50%-IL, the  
423 advantages of the sorbents described in this work are obvious even more when one  
424 considers that there is no need for organic solvents or thermal treatment for their  
425 synthesis. SSMMP are thus low-cost and energy expenditure sorbent materials.

426 Table 5- CO<sub>2</sub> sorption values for different inorganic silicate materials found in the  
427 literature

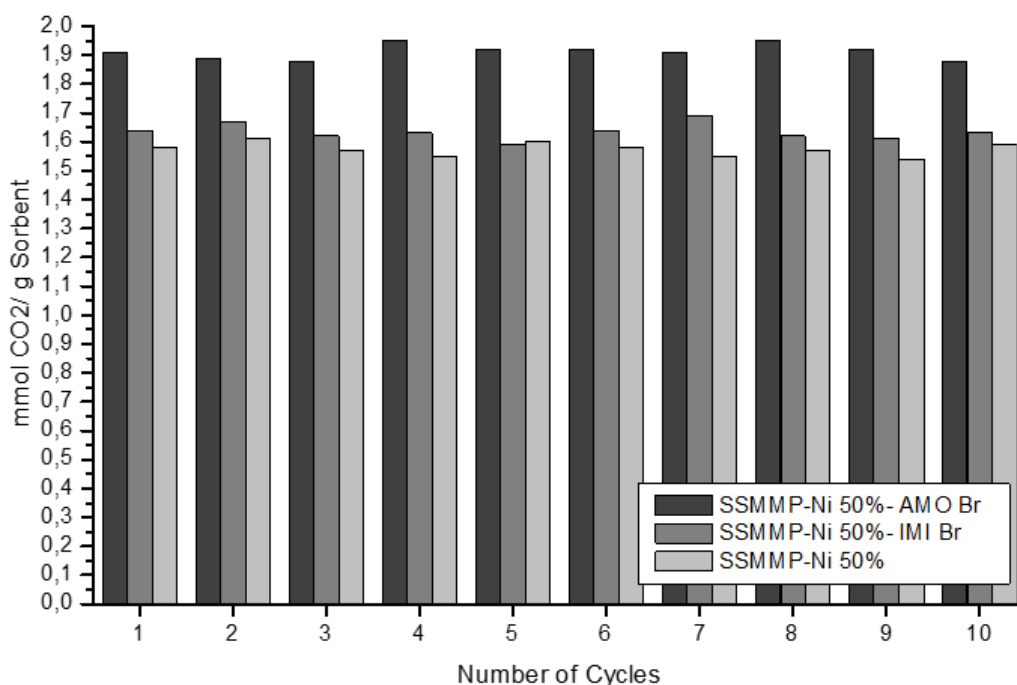
Sample	Analyses conditions	Sorption (mmol CO <sub>2</sub> /g)	N <sub>2</sub> /CO <sub>2</sub> selectivity	Ref.
Si-[P <sub>8883</sub> ]TFSI/SiO <sub>2</sub>	1 bar, 40°C	0.99	~6.0	[75]
SIL-15% - [C <sub>4</sub> TPI <sub>m</sub> ] [Cl]	4 bar, 45°C	1.45	2.7	[26]

SIL-15% - [i-C 5 TPIIm] [Cl]	4 bar,45°C	1.50	4.5	[26]
SiO <sub>2</sub> -Si - P <sub>4443</sub> BF <sub>4</sub>	1 bar,25°C	~0.60	8	[76]
SiO <sub>2</sub> -Si - P <sub>8883</sub> BF <sub>4</sub>	1 bar,25°C	~0.61	6	[76]
MCMRH-IL-A20	4 bar,25°C	1.25	-	[53]
MCMRH-IL-B10	4 bar,25°C	1.77	-	[53]
SSMMP-5%-Im(nBu)-I	1 bar,25°C	0.89	16.9	[7]
SMMP-5%-Im(nBu)-NTf <sub>2</sub>	1 bar,25°C	0.95	-	[7]
S-mBmim [Tf <sub>2</sub> N]-10	4 bar,45°C	~1.27	3.7	[77]
S-mBmim [Br]-10	4 bar,45°C	~1.67	4.8	[77]
ILCIM50	1 bar,25°C	0.75	-	[78]
MCM-41/[VBTMA][Cl]	1 bar,40°C	0.64	-	[29]
SIL-AAB-IL	1 bar,25°C	1.04	-	[79]
SIL-IB-IL	1 bar,25°C	0.61	-	[80]
MMT-BMIMCl-1-2.0	1 bar,30°C	0.40	-	[72]
SSMMP-Ni 50%-AMO Br	1 bar,25°C	1.91	13.1	This work
SSMMP-Ni 50%-IMI Br	1 bar,25°C	1.64	14.4	This work

428

### 429 3.3 Sorbents structural stability

430



431

432 Figure 9- Sorption/desorption CO<sub>2</sub> tests performed at 1 bar CO<sub>2</sub> pressure and 25°C.

433

434 Figure 9 presents the cyclability tests of CO<sub>2</sub> sorption/desorption for SSMMP-Ni 50%-  
435 AMO Br, SSMMP-Ni 50%-IMI-Br and SSMMP-Ni 50%. CO<sub>2</sub> sorption capacity was  
436 constant after 10 cycles of CO<sub>2</sub> sorption/desorption. FTIR analysis was performed on  
437 samples before and after the 10 cycles and no structural changes were observed. See  
438 supplementary material (S2).

### 439 **3.4 CO<sub>2</sub> cycloaddition in epoxide**

440 Table 5 presents the results for solvent-free cyclic carbonate syntheses using  
441 SSMMP-Ni X% and SSMMP-Ni 50%-IL as heterogeneous catalysts. Tests carried out  
442 with SSMMP-Ni 50% and SSMMP-Ni 50%-IL (Table 6, entries 3-9), with no cocatalyst  
443 addition (TBAB) presented a low propylene carbonate conversion. SSMMP-Ni 50%-IL  
444 low catalytic activity is probably due to the interaction between the IL and the acidic  
445 hydroxyl groups on the catalyst surface preventing the nucleophilic attack of the halide  
446 anion to the less hindered carbon of the epoxide molecule, at the same time as  
447 preventing CO<sub>2</sub> interaction with -SiOH, -MgOH and -NiOH groups [72,81,82]. Yet,  
448 SSMMP-Ni 50%-IMI Br, SSMMP-Ni 50%-IMI I, SSMMP-Ni 50%- AMO Br and SSMMP-  
449 Ni 50%- AMO I present a strong CO<sub>2</sub>/IL interaction (as seen in section 3.1), difficulting  
450 the IL/epoxide interaction, the epoxide ring opening and the subsequent CO<sub>2</sub> insertion  
451 into the epoxide ring and cyclic carbonate formation [27]. For ST-Ni 50% and SSMMP-  
452 Ni 50% (Table 6, entries 2 and 3), low catalytic activity was expected due to the lack  
453 of a nucleophilic agent in the catalyst [82]. The addition of TBAB as cocatalyst in the  
454 reactions with ST-Ni 50%, SSMMP-Ni 50% and SSMMP-Ni 100% (Table 6, entries 10,  
455 12-19), increased the catalytic activity. When comparing the catalytic performance of  
456 SSMMP-Ni 50% and ST-Ni 50% (Table 6), a drop of 24.5% in the propylene carbonate  
457 yield is observed. The low catalytic activity of ST-Ni 50% is attributed to the lower  
458 number of OH groups in the catalyst surface, due to heat treatment, allied to the  
459 difficulty of CO<sub>2</sub> interaction with the Lewis acid sites (Mg and Ni) of the octahedral layer  
460 of the lamellar structure of synthetic talc. Comparing samples containing 0%, 50% and  
461 100% of Ni replacing Mg in the octahedral structure (Table 6, entries 11, 12 and 18,  
462 respectively), an increase of 31.2 % in carbonate yield was observed when 50% of Mg  
463 was replaced by Ni. When 100% of Mg was replaced by Ni no significant increase in  
464 propylene carbonate yield was observed. Aiming to evaluate the possibility of using  
465 the same material as sorbent/catalyst, a cycloaddition reaction using SSMMP-50%-R  
466 (Table 6, entry 16) previously used in the CO<sub>2</sub> sorption, CO<sub>2</sub>/N<sub>2</sub> separation, and

467 submitted to 10 CO<sub>2</sub> sorption/desorption cycles was tested as catalyst. When  
 468 comparing the result of bare SSMMP-Ni 50% with reused SSMMP-Ni 50%-R, a similar  
 469 propylene carbonate yield was obtained. This result reveals the possibility of reusing  
 470 SSMMP-Ni X% as heterogeneous catalysts after they are used as solid sorbent in CO<sub>2</sub>  
 471 capture. Structural analysis of the SSMMP-Ni 50%-R was performed before and after  
 472 it was used as a catalyst showing no changes as seen in Figure S2.

473

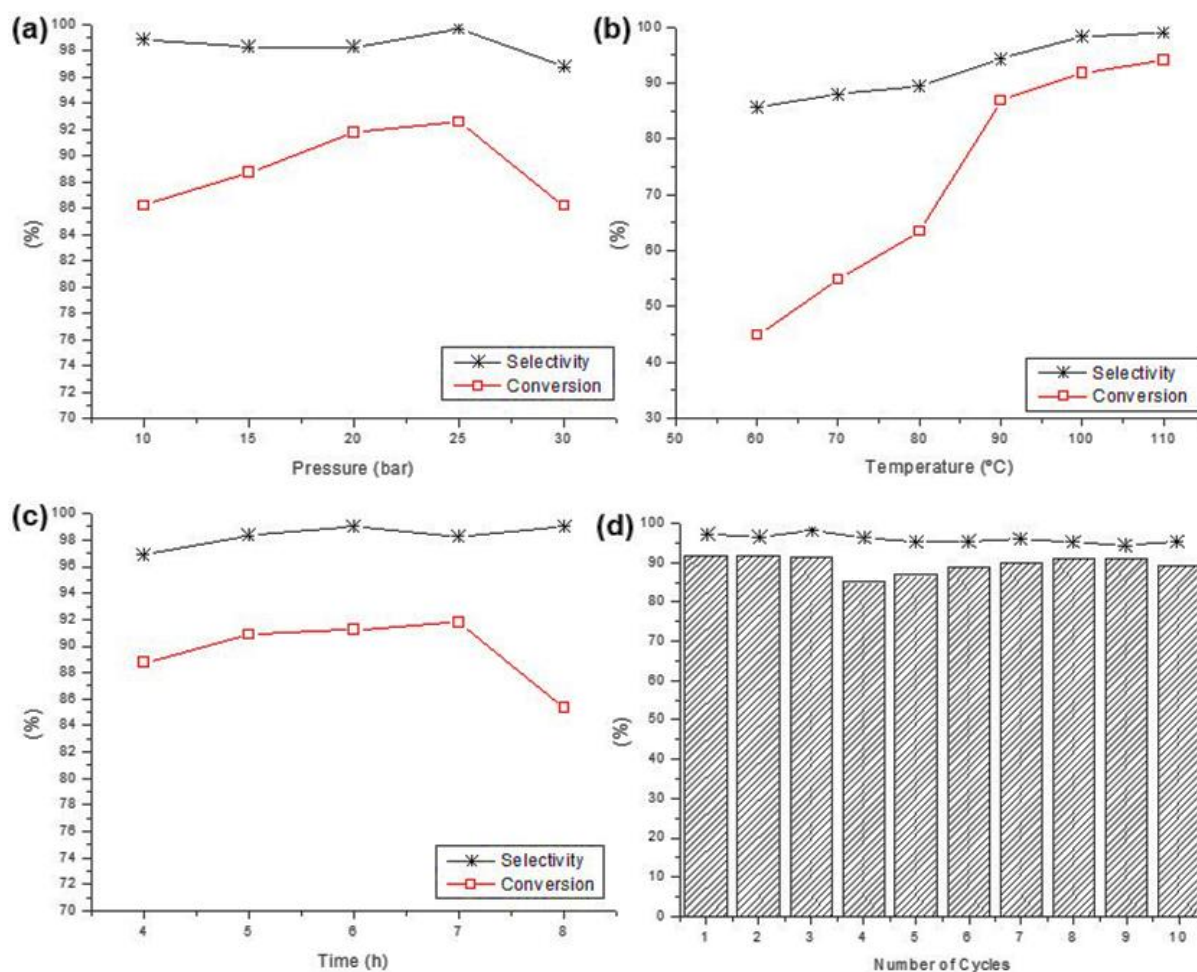
474 Table 6- Catalytic performance of synthesized materials in the cyclic propylene  
 475 carbonate syntheses.

Entry	Sample	Cocat.	Conversion (%)	Selectivity (%)	Yield (%)
1	TBAB <sup>(a)</sup>	-----	35.6	97.1	35
2	ST-Ni 50% <sup>(a)</sup>	-----	9.8	-	-
3	SSMMP-Ni 50% <sup>(a)</sup>	-----	9.3	-	-
4	SSMMP-Ni 50%-AMO Br <sup>(a)</sup>	-----	5.5	-	-
5	SSMMP-Ni 50%-AMO Cl <sup>(a)</sup>	-----	3.7	-	-
6	SSMMP-Ni 50%-AMO I <sup>(a)</sup>	-----	2.9	-	-
7	SSMMP-Ni 50%-IMI Br <sup>(a)</sup>	-----	6.7	-	-
8	SSMMP-Ni 50%-IMI Cl <sup>(a)</sup>	-----	13.5	-	-
9	SSMMP-Ni 50%-IMI I <sup>(a)</sup>	-----	7.2	-	-
10	ST-Ni 50% <sup>(a)</sup>	TBAB	72.6	90.9	65.7
11	SSMMP(0%Ni) <sup>(a)</sup>	TBAB	60.0	98.4	59.0
12	SSMMP-Ni 50% <sup>(a)</sup>	TBAB	91.8	98.3	90.4
13	SSMMP-Ni 50% <sup>(b)</sup>	TBAB	86.2	94.3	81.2
14	SSMMP-Ni 50% <sup>(c)</sup>	TBAB	94.2	99.0	93.3
15	SSMMP-Ni 50% <sup>(d)</sup>	TBAB	88.8	98.3	87.3
16	SSMMP-Ni 50%-R* <sup>(e)</sup>	TBAB	93.6	96.1	89.9
17	SSMMP-Ni 50% <sup>(f)</sup>	TBAB	86.5	98.7	85.3
18	SSMMP-Ni 100% <sup>(a)</sup>	TBAB	96.6	93.2	90.0
19	SSMMP-Ni 100% <sup>(d)</sup>	TBAB	91.1	95.2	86.7

Reactional conditions: <sup>(a)</sup>20 bar, 100°C and 7h; <sup>(b)</sup>20bar, 90°C and 7h; <sup>(c)</sup>20 bar, 110°C and 7h; <sup>(d)</sup>15 bar, 100°C and 7h; <sup>(e)</sup>SSMMP-Ni 50% after 10 sorption/desorption CO<sub>2</sub> cycles; <sup>(f)</sup>20 bar, 90°C and 5h; 0.1 mol EP, TBAB 0.6 mol% of PE and 0.2 g of catalyst.

476 SSMMP-Ni 50% stability and reaction conditions effect (pressure, temperature and  
 477 reaction time) on the catalytic performance in propylene carbonate synthesis was  
 478 evaluated (Figure 10, (a), (b) and (c). CO<sub>2</sub> pressure variation (10-30 bar) was  
 479 performed at 100°C and 7 hours of reaction time. As seen in Figure 10 (a), when  
 480 increasing the CO<sub>2</sub> pressure from 10 to 25 bar, a subtle increase in the propylene  
 481 carbonate yield is observed, from 86.2% to 92.0%. However, when increasing CO<sub>2</sub>  
 482 pressure to 30 bar, the cyclic carbonate yield drops from 92.0% to 86.1%, indicating

483 that at higher CO<sub>2</sub> pressures the catalytic activity of SSMMP-Ni 50% decreases. The  
 484 effect of temperature was evaluated by maintaining 20 bar of CO<sub>2</sub> pressure and a  
 485 reaction time of 7 hours and varying the reaction temperature from 60°C to 110°C. The  
 486 temperature elevation increased the cyclic propylene carbonate yield from 44.8% to  
 487 93.3%, respectively proving the influence of temperature on the catalytic activity of  
 488 SSMMP-Ni 50%. The variation of the reaction time (2-7 h) was carried out keeping the  
 489 temperature of 100°C and 20 bar of CO<sub>2</sub> pressure. Increasing reaction time from 2 h to  
 490 4 h increases catalytic activity and propylene carbonate yield from 59.4% to 85.9%,  
 491 respectively. After 4 hours of reaction time, the carbonate yield becomes stable,  
 492 showing a slight increase until reaching a yield of 90.4% after 7 hours. Based on the  
 493 results described above, a synthesis under reaction conditions of 20 bar, 90°C and 5  
 494 hours was carried out (Table 6, entry 17) and a yield of 85.3% of propylene carbonate  
 495 was obtained, showing that reaction conditions of 20 bar, 100°C and 7 hours as ideal.



497 Figure 10- Evaluation of reactional condition variation effect in cyclic propylene  
498 carbonate syntheses and cycles of sorption/desorption using SSMMP-Ni 50%: effect  
499 of (a) pressure, (b) temperature, (c) reaction time and (d) number of cycles.

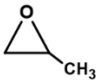
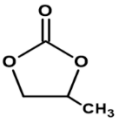
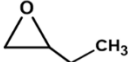
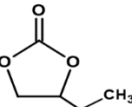
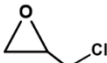
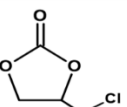
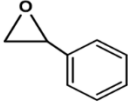
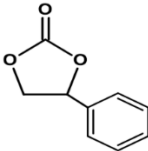
500

501 The stability of SSMMP-Ni 50% used as catalyst was investigated using the same  
502 sample for 10 consecutive reaction cycles, under reaction conditions of 20 bar, 100 °C  
503 and 7h. As seen in Figure 10 (d), conversion and selectivity are constant indicating the  
504 high stability of the SSMMP-Ni 50% as catalyst in cycloaddition reaction. A structural  
505 investigation of the catalyst was performed by infrared spectroscopy before and after  
506 the 10 cycles and the spectrograms are shown in Figure S3. The catalyst structure is  
507 unaltered, being visible cocatalyst residue remaining after water washing.

508 The catalytic performance of SSMMP-Ni 50% in the cycloaddition reaction using 3 new  
509 substrates was investigated (Table 7). The reactions were carried out using TBAB as  
510 cocatalyst (0.6 mol% of the substrate), at 20 bar of CO<sub>2</sub> pressure, at 100°C of  
511 temperature, for 7h. SSMMP-Ni 50% presents a good catalytic performance for all  
512 cyclic carbonate syntheses, as seen in Table 7. This behavior differs from some results  
513 described in the literature, reporting the drop in the cyclic carbonate yield with the  
514 increase of the side chain linked to the epoxide ring. This behavior is attributed to the  
515 hysterical hindering caused by the molecule size making it difficult the interaction of  
516 the catalyst active sites with the epoxide molecule [82]. Among the tested substrates,  
517 the highest yield was found for 1,2-butylene carbonate (85.2%) and the lowest for  
518 chloropropene carbonate (92.9%) due to the low selectivity of the reaction.

519 Table 7- Catalytic performance of SSMMP-Ni 50% in addition cycle reactions with  
520 different epoxides



Reagent	Product	Selectivity	Yield (%)
		98.3	90.4
		87.1	85.2
		99.9	92.9
		99.9	90.1

521

522 Table 8 presents, for comparison, results from the literature on the catalytic  
523 performance of natural phyllosilicates and layered double hydroxide (LDH). When  
524 comparing the synthesis (or preparation) steps of materials described in the literature  
525 to this work, it can be highlighted that, unlike the other catalysts, in the SSMMP-Ni 50%  
526 synthesis no organic solvents are needed for material exfoliation nor calcination at high  
527 temperatures since SSMMP is obtained prior to the formation of the organized and  
528 lamellar structure of synthetic talc, before the hydrothermal treatment. At this stage,  
529 SSMMP-Ni X% have reactive groups (Si-OH, Ni-OH, and Mg-OH) distributed across  
530 their surface. These groups make it easier for the material to interact with CO<sub>2</sub>,  
531 epoxide, and other reagents, and also facilitate their functionalization. Regarding  
532 reaction conditions, the use of moderate reaction conditions without the need for  
533 organic solvents during the addition cycle reactions for SSMMP should be highlighted.  
534 The high and easy reuse of SSMMP-Ni 50%, with no drop in conversion and selectivity,  
535 is another indicator of the good potential of these materials as heterogeneous  
536 catalysts.

537

Table 8- Comparing the catalytic behavior of different materials

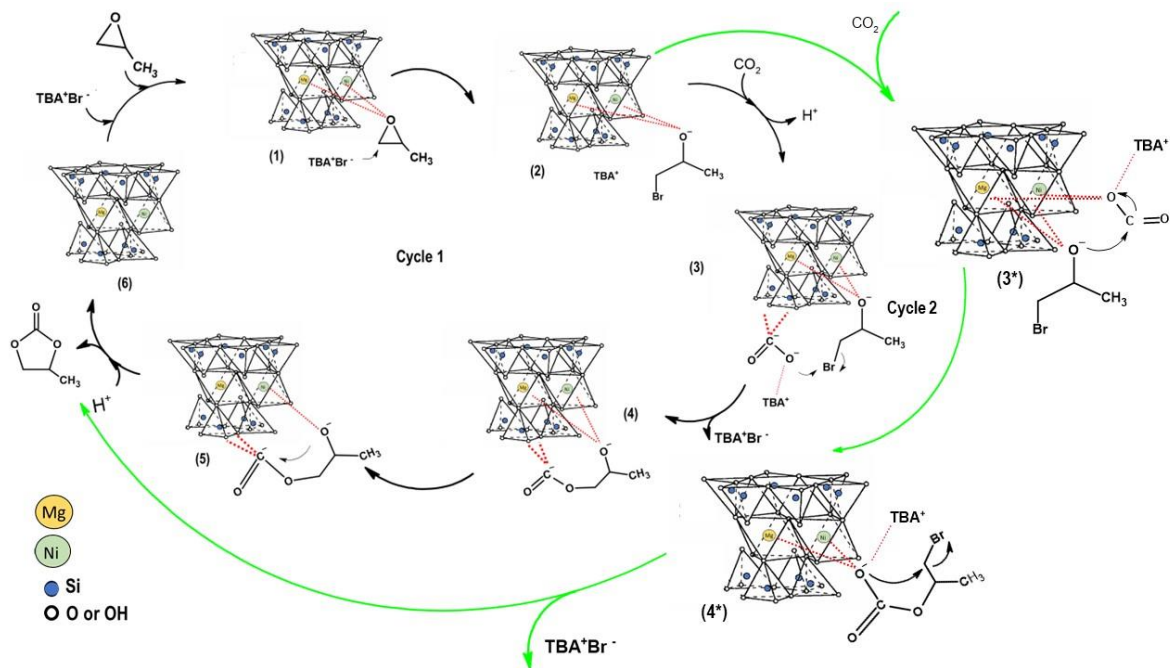
Catalyst	Cocatalyst / Solvent	Reaction conditions	Yield (%)	Ref.
Talc <sup>(a)</sup>	TBAB / CH <sub>3</sub> CN	140°C, 30 bar, 20h	92.7	[83]
Biotite <sup>(a)</sup>	TBAB / CH <sub>3</sub> CN	120°C, 20 bar, 20h	30.4	[83]
Chlorite <sup>(a)</sup>	TBAB / CH <sub>3</sub> CN	120°C, 20 bar, 20h	38.7	[83]
Phlogopite <sup>(a)</sup>	TBAB / CH <sub>3</sub> CN	120°C, 20 bar, 20h	35.0	[83]
Vermiculite <sup>(a)</sup>	TBAB / CH <sub>3</sub> CN	150°C, 30 bar, 20h	86.8	[83]

slagLDH(600) <sup>(b)</sup>	- / DMF	100°C, 1 bar, 48h	90.0	[84]
MgFeAl-LDH (WE) <sup>(c)</sup>	TBAB / -	50°C, 5 bar, 7h	96.2	[82]
Montmorillonite <sup>(b)</sup>	TBAB / -	100°C, 1 bar, 24h	--	[85]
slagHC(Cl)(800) <sup>(b)</sup>	- / DMF	100°C, 1 bar, 24h	85	[86]
Smectite-Mg-Na-K-4 <sup>(a)</sup>	- / -	150°C, 80 bar, 15h	80.7	[87]
SSMMP-Ni 50% <sup>(a)</sup>	TBAB / -	100°C, 20 bar, 7h	90.4	This work

<sup>(a)</sup> Propylene epoxide; <sup>(b)</sup> Styrene epoxide; <sup>(c)</sup> Epichlorohydrin.

### 538 3.1 Proposed catalytic mechanism

539 Figure 11 presents a catalytic mechanism proposition based on previously described  
540 works in the literature [81,82]. The main catalytic route involves metal ions (Mg and Ni)  
541 acting as Lewis's acid activators attracting the epoxide ring oxygen to bind to them.  
542 The bromide anion (Br<sup>-</sup>) of the nucleophile TBAB attacks the least hindered carbon of  
543 the epoxide ring (1) to form the oxyanion intermediate (2). Simultaneously, the  
544 electron-rich oxygen atom of the groups (-MgOH and -SiOH) reacts with CO<sub>2</sub> leading  
545 to the formation of the carbonate anion, after the O<sup>-</sup> of the carbonate anion attacks the  
546 bromine-anchored carbon atom (3) dissociating the C-Br bond (4). Finally, the  
547 corresponding cyclic carbonate can be produced by closing the intramolecular ring (5),  
548 and the catalyst is regenerated to the next epoxide molecule (6). A second catalytic  
549 cycle is probably occurring simultaneously, but less probable to be occurring due to  
550 the competition of epoxide and CO<sub>2</sub> for the interaction with metal ions. The proposed  
551 catalytic route starts with CO<sub>2</sub> adsorbed by the Lewis acid metal ions (Mg and Ni) of  
552 the SSMMP-Ni 50% (3\*), resulting in the intermolecular nucleophilic addition of the  
553 oxy-anion intermediate to form a metal carbonate intermediate (4\*). Then next,  
554 intramolecular ring closure of the carbonate anion intermediate (5), yields the  
555 corresponding cyclic carbonate as in cycle 1, and catalyst regeneration occurs.  
556



#### 560 4. Conclusion

561 In this work, we report the synthesis, characterization and use of synthetic silico-  
562 metallic mineral particles (SSMMP-Ni) and SSMMP-Ni functionalized with IL.  
563 These materials proved to be highly efficient stable (1) solid adsorbents in CO<sub>2</sub>  
564 capture from CO<sub>2</sub>/N<sub>2</sub> gas mixtures, (2) heterogeneous catalysts in the solvent-  
565 free cyclic carbonates synthesis, with easy catalyst/product separation. SSMMP-  
566 Ni 50%-AMO Br showed the best performance of CO<sub>2</sub> sorption, reaching 1.91  
567 mmol of CO<sub>2</sub>/g at 1 bar and 8.22 mmol of CO<sub>2</sub>/g at 30 bar. For CO<sub>2</sub>/N<sub>2</sub> separation,  
568 SSMMP-Ni 50%-IMI Br showed the highest selective capacity (14.4). It was  
569 evidenced that both the IL anion and cation influence the sorption capacity and  
570 selectivity. The ammonium cation is more efficient in capturing CO<sub>2</sub> and  
571 imidazolium is more selective for capturing CO<sub>2</sub> in CO<sub>2</sub>/N<sub>2</sub> mixture. Among the  
572 anions, Br<sup>-</sup> presents the highest interaction energy with CO<sub>2</sub>, presenting better  
573 performance both for pure CO<sub>2</sub> sorption and CO<sub>2</sub> selectivity. In catalysis, the  
574 sample containing 50% of Ni replacing Mg, presented the best catalytic  
575 performance, reaching conversion and selectivity in propylene carbonate  
576 production superior to 90%. It was also evidenced the possibility of reusing the  
577 SSMMP-Ni 50%-R sample as a catalyst in the synthesis of cyclic carbonates,  
578 after was used in 10 cycles of CO<sub>2</sub> sorption/desorption, evidencing the possibility  
579 of this material being used in CO<sub>2</sub> capture and transformation. The easy synthesis  
580 of these materials (one-pot), using low-cost reagents, without the use of organic  
581 solvents and with low energy expenditure, allied to the good results presented in  
582 this work, point to the potential of the use of SSMMP in the industry both in CO<sub>2</sub>  
583 capture in post-combustion process, as well as in chemical transformation after  
584 its capture.

585

#### 586 Acknowledgment

587 This study was written by some members of the Capes- PRINT  
588 Internationalization Project from PUCRS University and was financed in part by  
589 the Coordination for the Improvement of Higher Education Personnel- Brasil  
590 (CAPES) – Finance Code 001. Sandra Einloft thanks CNPq for the research  
591 scholarship.

592 **Bibliography**

- 593 [1] O. Tursunov,, L. Kustov,, A. Kustov, *Oigyl & Gas Science and Technology*  
594 72(2017) (2019) 1–9. 10.2516/ogst/2017027.
- 595 [2] I.H. Arellano,, S.H. Madani,, J. Huang,, P. Pendleton, *Chemical*  
596 *Engineering Journal* 283 (2016) 692–702. 10.1016/j.cej.2015.08.006.
- 597 [3] B. Ozcan,, E. Gultekin, *Eurasian Journal of Business and Economics* 9(18)  
598 (2016) 113–34. 10.17015/ejbe.2016.018.07.
- 599 [4] M.T. Ravanchi,, S. Sahebdehfar, *Process Safety and Environmental*  
600 *Protection* 145 (2021) 172–94. 10.1016/j.psep.2020.08.003.
- 601 [5] R.M. Cuéllar-Franca,, A. Azapagic, *Journal of CO2 Utilization* 9 (2015) 82–  
602 102. 10.1016/j.jcou.2014.12.001.
- 603 [6] M. Younas,, M. Rezakazemi,, M. Daud,, M.B. Wazir,, S. Ahmad,, N. Ullah,,  
604 Inamuddin,, S. Ramakrishna, *Progress in Energy and Combustion Science*  
605 80 (2020). 10.1016/j.pecs.2020.100849.
- 606 [7] D. Rodrigues,, F. Bernard,, C. Le,, E. Duarte,, P. Micoud,, A. Castillo,, F.  
607 Martin,, S. Einloft, *Applied Clay Science* 226(May) (2022) 106572.  
608 10.1016/j.clay.2022.106572.
- 609 [8] B. Li,, Y. Duan,, D. Luebke,, B. Morreale, *Applied Energy* 102 (2013) 1439–  
610 47. 10.1016/j.apenergy.2012.09.009.
- 611 [9] J. Wang,, D. Kong,, J. Chen,, F. Cai,, L. He, *Journal of Molecular Catalysis*  
612 *A: Chemical* 249 (2006) 143–8. 10.1016/j.molcata.2006.01.008.
- 613 [10] D. Rodrigues,, L.G. Hunter,, F.L. Bernard,, M.F. Rojas,, F. Dalla Vecchia,,  
614 S. Einloft, *Catalysis Letters* 149(3) (2019) 733–43. 10.1007/s10562-018-

- 615 2637-4.
- 616 [11] J. Ma,, J. Liu,, Z. Zhang,, B. Han, *Green Chemistry* 14(9) (2012) 2410–20.  
617 10.1039/c2gc35711a.
- 618 [12] B.M. Bhanage,, S.I. Fujita,, Y. Ikushima,, K. Torii,, M. Arai, *Green*  
619 *Chemistry* 5(1) (2003) 71–5. 10.1039/b207750g.
- 620 [13] K. Yamaguchi,, K. Ebitani,, T. Yoshida, *Journal American Chemical Society*  
621 121 (1999) 4526–7. 10.1021/ja9902165.
- 622 [14] M.F. Rojas,, F.L. Bernard,, A. Aquino,, J. Borges,, F.D. Vecchia,, S.  
623 Menezes,, R. Ligabue,, S. Einloft, *Journal of Molecular Catalysis A:*  
624 *Chemical* 392 (2014) 83–8. 10.1016/j.molcata.2014.05.007.
- 625 [15] T. Yano,, H. Matsui,, T. Koike,, H. Ishiguro,, H. Fujihara,, M. Yoshihara,, T.  
626 Maeshima, *Chemical Communications* 2(12) (1997) 1129–30.  
627 10.1039/a608102i.
- 628 [16] J.L. Jiang,, R. Hua, *Synthetic Communications* 7911(36) (2006) 3141–  
629 3148. 10.1080/00397910600908744.
- 630 [17] J. Wang,, J. Wu,, N. Tang, *Inorganic Chemistry Communications* 10(12)  
631 (2007) 1493–5. 10.1016/j.inoche.2007.09.022.
- 632 [18] C. Martín,, G. Fiorani,, A.W. Kleij, *ACS Catalysis* 5(2) (2015) 1353–70.  
633 10.1021/cs5018997.
- 634 [19] Y. Sun,, H. Huang,, H. Vardhan,, B. Aguila,, C. Zhong,, J.A. Perman,, A.M.  
635 Al-Enizi,, A. Nafady,, S. Ma, *ACS Applied Materials and Interfaces* 10(32)  
636 (2018) 27124–30. 10.1021/acsami.8b08914.
- 637 [20] F. Nocito,, A. Dibenedetto, *Current Opinion in Green and Sustainable*

- 638 Chemistry 21 (2020) 34–43. 10.1016/j.cogsc.2019.10.002.
- 639 [21] N. Aini,, M. Razali,, K.T. Lee,, S. Bhatia,, A. Rahman, Renewable and  
640 Sustainable Energy Reviews 16(7) (2012) 4951–64.  
641 10.1016/j.rser.2012.04.012.
- 642 [22] A. Hafiidz,, M. Fauzi,, N. Aishah,, S. Amin, Renewable and Sustainable  
643 Energy Reviews 16(8) (2012) 5770–86. 10.1016/j.rser.2012.06.022.
- 644 [23] W. Cheng,, Q. Su,, J. Wang,, J. Sun,, F.T.T. Ng, Catalysts 3(4) (2013) 878–  
645 901. 10.3390/catal3040878.
- 646 [24] F.L. Bernard,, D.M. Rodrigues,, B.B. Polesso,, A.J. Donato,, M. Seferin,, V.  
647 V. Chaban,, F.D. Vecchia,, S. Einloft, Fuel Processing Technology 149  
648 (2016) 131–8. 10.1016/j.fuproc.2016.04.014.
- 649 [25] B. Monteiro,, R. Nabais,, A.A. Paz,, L. Cabrita,, L.C. Branco,, I.M.  
650 Marrucho,, L.A. Neves,, C.L. Pereira, Energy Tech (2017) 2158–62.  
651 10.1002/ente.201700228.
- 652 [26] R. Duczinski,, B.B. Polesso,, F.L. Bernard,, H.Z. Ferrari,, P.L. Almeida,,  
653 M.C. Corvo,, E.J. Cabrita,, S. Menezes,, S. Einloft, Journal of  
654 Environmental Chemical Engineering 8(3) (2020) 103740.  
655 10.1016/j.jece.2020.103740.
- 656 [27] D.M. Rodrigues,, L.M. dos Santos,, F.L. Bernard,, I.S. Pinto,, R. Zampiva,,  
657 G. Kaufmann,, S. Einloft, SN Applied Sciences 2(12) (2020) 1–11.  
658 10.1007/s42452-020-03712-z.
- 659 [28] S. Udayakumar,, M.K. Lee,, H.L. Shim,, S.W. Park,, D.W. Park, Catalysis  
660 Communications 10(5) (2009) 659–64. 10.1016/j.catcom.2008.11.017.

- 661 [29] F. Nkinahamira,, T. Su,, Y. Xie,, G. Ma,, H. Wang,, J. Li, 326 (2017) 831–  
662 8. 10.1016/j.cej.2017.05.173.
- 663 [30] J. Sun,, W. Cheng,, W. Fan,, Y. Wang,, Z. Meng,, S. Zhang, Catalysis  
664 Today 148(3–4) (2009) 361–7. 10.1016/j.cattod.2009.07.070.
- 665 [31] T. Sakai,, Y. Tsutsumi,, T. Ema, Green Chemistry 10 (2008) 337–41.  
666 10.1039/b718321f.
- 667 [32] A. Dindi,, D.V. Quang,, L.F. Vega,, E. Nashef,, M.R.M. Abu-Zahra, Journal  
668 of CO<sub>2</sub> Utilization 29(November 2018) (2019) 82–102.  
669 10.1016/j.jcou.2018.11.011.
- 670 [33] A. Dumas,, M. Mizrahi,, F. Martin,, F. Requejo, 15 (2015) 5451–5463.  
671 10.1021/acs.cgd.5b01076.
- 672 [34] M. Claverie,, A. Dumas,, C. Carême,, M. Poirier,, C. Le Roux,, P. Micoud,,  
673 F. Martin,, C. Aymonier, Chemistry - A European Journal 24(3) (2018) 519–  
674 42. 10.1002/chem.201702763.
- 675 [35] K.E. Bremmell,, J. Addai-Mensah, Journal of Colloid and Interface Science  
676 283(2) (2005) 385–91. 10.1016/j.jcis.2004.09.048.
- 677 [36] F. Martin,, C. Aymonier,, S. Einloft,, C. Carême,, M. Poirier,, M. Claverie,,  
678 M.A. Prado,, G. Dias,, C. Quilfen,, G. Aubert,, P. Micoud,, C. Le Roux,, S.  
679 Salvi,, A. Dumas,, S. Féry-Forgues, Journal of Geochemical Exploration  
680 200(February) (2019) 27–36. 10.1016/j.gexplo.2019.02.002.
- 681 [37] A. Dumas,, C. Le Roux,, F. Martin,, P. Micoud, METHOD FOR  
682 PREPARING A HYDROGEL COMPRISING SILICO-METALLIC MINERAL  
683 PARTICLES AND HYDROGEL WO2013093339 A1. WO 2013093339 A1,  
684 2013.



- 685 [38] A. Dumas,, F. Martin,, E. Ferrage,, P. Micoud,, C. Le Roux,, S. Petit,  
686 Applied Clay Science 85(1) (2013) 8–18. 10.1016/j.clay.2013.09.006.
- 687 [39] F.L. Bernard,, R.B. Duczinski,, M.F. Rojas,, M.C.C. Fialho,, L.Á. Carreño,,  
688 V. V. Chaban,, F.D. Vecchia,, S. Einloft, Fuel 211 (2018) 76–86.  
689 10.1016/j.fuel.2017.09.057.
- 690 [40] M. Rojas,, L. Pacheco,, A. Martinez,, K. Pradilla,, F. Bernard,, S. Einloft,,  
691 L.A. Carre, 452 (2017). 10.1016/j.fluid.2017.08.026.
- 692 [41] W.J. Koros,, D.R. Paul, Journal of Polymer Science: Polymer Physics  
693 Edition 14(10) (1976) 1903–7. 10.1002/pol.1976.180141014.
- 694 [42] A. Azimi,, M. Mirzaei, Chemical Engineering Research and Design 111  
695 (2016) 262–8. 10.1016/j.cherd.2016.05.005.
- 696 [43] M. Fernández Rojas,, L. Pacheco Miranda,, A. Martinez Ramirez,, K.  
697 Pradilla Quintero,, F. Bernard,, S. Einloft,, L.A. Carreño Díaz, Fluid Phase  
698 Equilibria (2017) 103–12. 10.1016/j.fluid.2017.08.026.
- 699 [44] M.G. Da Fonseca,, C.R. Silva,, J.S. Barone,, C. Airoldi, Journal of Materials  
700 Chemistry 10(3) (2000) 789–95. 10.1039/a907804e.
- 701 [45] E. Bahri,, S. Dikmen,, A. Yildiz,, R. Gören,, Ö. Elitok, Turkish Journal of  
702 Earth Sciences 22(4) (2013) 632–44. 10.3906/yer-1112-14.
- 703 [46] G. Dias,, M.A. Prado,, C. Carone,, R. Ligabue,, A. Dumas,, F. Martin,, C.  
704 Le Roux,, P. Micoud,, S. Einloft, Polymer Bulletin 72(11) (2015) 2991–  
705 3006. 10.1007/s00289-015-1449-6.
- 706 [47] P. Schroeder, CMS Workshop Lectures 11(October) (2002) 181–206.
- 707 [48] M.A. Prado,, G. Dias,, C. Carone,, R. Ligabue,, A. Dumas,, C. Le Roux,, P.

- 708 Micoud,, F. Martin,, S. Einloft, *Journal of Applied Polymer Science* 132(16)  
709 (2015) 1–8. 10.1002/app.41854.
- 710 [49] G. Dias,, M. Prado,, C. Carone,, R. Ligabue,, A. Dumas,, C. Le Roux,, P.  
711 Micoud,, F. Martin,, S. Einloft, *Macromolecular Symposia* 367(1) (2016)  
712 136–42. 10.1002/masy.201500141.
- 713 [50] F. Martin,, P. Micoud,, P. Sabatier,, A.J. Guesde,, A.J. Guesde,, P.  
714 Sabatier, *Can. Mineral* 37 (1999) 997–1006.
- 715 [51] K. Chabrol,, M. Gressier,, N. Pebere,, M.J. Menu,, F. Martin,, J.P. Bonino,,  
716 C. Marichal,, J. Brendle, *Journal of Materials Chemistry* 20(43) (2010)  
717 9695–706. 10.1039/c0jm01276a.
- 718 [52] S. Mor,, C.K. Manchanda,, S.K. Kansal,, K. Ravindra, *Journal of Cleaner*  
719 *Production* 143 (2017) 1284–90. 10.1016/j.jclepro.2016.11.142.
- 720 [53] R. Duczinski,, F. Bernard,, M. Rojas,, E. Duarte,, V. Chaban,, F.D.  
721 Vecchia,, S. Menezes,, S. Einloft, *Journal of Natural Gas Science and*  
722 *Engineering* 54(January) (2018) 54–64. 10.1016/j.jngse.2018.03.028.
- 723 [54] K.A. Carrado,, L. Xu,, R. Csencsits,, J. V Muntean, *American Chemical*  
724 *Society* (5) (2001) 3766–73.
- 725 [55] M.G. da Fonseca,, C. Airoidi, *Materials Research Bulletin* 36(1–2) (2001)  
726 277–87. 10.1016/S0025-5408(00)00470-0.
- 727 [56] K. Fujii,, S. Hayashi, *Applied Clay Science* 29(3–4) (2005) 235–48.  
728 10.1016/j.clay.2005.01.005.
- 729 [57] J.T. Klopogge, *Raman Spectroscopy of Clay Minerals*, Vol. 8, first ed.,  
730 Elsevier Ltd., 2017.

- 731 [58] J. Grondin,, J. Lass,, T. Buffeteau,, R. Holomb, Raman Spectroscopy  
732 2010(June 2010) (2011) 733–43. 10.1002/jrs.2754.
- 733 [59] M. Klein,, H. Squire,, B. Gurkan, Physical Chemistry C 124(1) (2020)  
734 5613–5623. 10.1021/acs.jpcc.9b08016.
- 735 [60] K. Noack,, P.S. Schulz,, N. Paape,, J. Kiefer, Physical Chemistry Chemical  
736 Physics 12 (2010) 14153–61. 10.1039/c0cp00486c.
- 737 [61] M.A. Prado,, G. Dias,, L.M. dos Santos,, R. Ligabue,, M. Poirier,, C. Le  
738 Roux,, P. Micoud,, F. Martin,, S. Einloft, SN Applied Sciences 2(6) (2020)  
739 1–13. 10.1007/s42452-020-2852-7.
- 740 [62] C.R. Silva,, M.G. Fonseca,, J.S. Barone,, C. Airoidi, Chemistry of Materials  
741 14(1) (2002) 175–9. 10.1021/cm010474c.
- 742 [63] A. Dumas,, F. Martin,, C. Le Roux,, P. Micoud,, S. Petit,, E. Ferrage,, J.  
743 Brendlé,, O. Grauby,, M. Greenhill-Hooper, Physics and Chemistry of  
744 Minerals 40(4) (2013) 361–73. 10.1007/s00269-013-0577-5.
- 745 [64] E. V Borodina,, F. Roessner,, S.I. Karpov,, V.F. Selemenev,  
746 NANOTECHNOLOGIES IN RUSSIA 5 (2010) 808–16.  
747 10.1134/S1995078010110091.
- 748 [65] M.S. Sader,, M. Ferreira,, M.L. Dias, Polímeros 16(1) (2006) 12–8.  
749 10.1590/s0104-14282006000100006.
- 750 [66] S. Park,, B. Seo,, D. Shin,, K. Kim,, W. Choi, Chemical Engineering Journal  
751 433(P1) (2022) 134486. 10.1016/j.cej.2021.134486.
- 752 [67] R.T. Tran,, E. Naseri,, A. Kolasnikov,, X. Bai,, J. Yang, Biotechnology and  
753 Applied Biochemistry 58 (2011) 335–44. 10.1002/bab.44.

- 754 [68] R. Malherbe,, R. Estrella,, F. Linares, The Journal Physical Chemistry C  
755 114 (41) (2010) 17773–87. <https://doi.org/10.1021/jp107754g>.
- 756 [69] J. Tang,, Y. Shen,, M. Radosz,, W. Sun, Industrial and Engineering  
757 Chemistry Research 48(30) (2009) 9113–8.
- 758 [70] J. Tang,, W. Sun,, H. Tang,, M. Radosz,, Y. Shen, American Chemical  
759 Society 38 (2005) 2037–9.
- 760 [71] S. Yamini Sudha,, A. Khanna, World Academy of Science, Engineering and  
761 Technology 33 (2009) 539–42.
- 762 [72] Y. Zhou,, J. Liu,, M. Xiao,, Y. Meng,, L. Sun, (2016).  
763 10.1021/acsami.5b11249.
- 764 [73] Y. Zhou,, J. Liu,, M. Xiao,, Y. Meng,, L. Sun, ACS Applied Materials and  
765 Interfaces 8(8) (2016) 5547–55. 10.1021/acsami.5b11249.
- 766 [74] I. Harvey,, S.H. Madani,, J. Huang,, P. Pendleton, CHEMICAL  
767 ENGINEERING JOURNAL 283 (2016) 692–702.  
768 10.1016/j.cej.2015.08.006.
- 769 [75] J. Zhu,, B. He,, J. Huang,, C. Li,, T. Ren, Microporous and Mesoporous  
770 Materials 260(July 2017) (2018) 190–200.  
771 10.1016/j.micromeso.2017.10.035.
- 772 [76] J. Zhu,, F. Xin,, J. Huang,, X. Dong,, H. Liu, Chemical Engineering Journal  
773 246 (2014) 79–87. 10.1016/j.cej.2014.02.057.
- 774 [77] B. Polesso,, R. Duczinski,, F.L. Bernard,, H.Z. Ferrari,, F.D. Vecchia,, S.  
775 Maria,, S. Einloft, Materials Research 22 (2019) 1–10.
- 776 [78] A. Aquino,, F. Bernard,, R. Ligabue,, M. Seferin,, V. V Chaban,, E.J.

777 Cabrita,, S. Einloft, Royal Society of Chemistry 5 (2015) 64220–7.  
778 10.1039/c5ra07561k.

779 [79] K. Helene,, F. Rasmus,, R. Anders, 55(8) (2012) 1648–56.  
780 10.1007/s11426-012-4683-x.

781 [80] V. Hiremath,, A.H. Jadhav,, H. Lee,, S. Kwon,, J. Gil, Chemical Engineering  
782 Journal 287 (2016) 602–17. 10.1016/j.cej.2015.11.075.

783 [81] F. Lagarde,, H. Srour,, N. Berthet,, N. Oueslati,, B. Bousquet,, A. Nunes,,  
784 A. Martinez,, V. Dufaud, Journal of CO2 Utilization 34(June) (2019) 34–9.  
785 10.1016/j.jcou.2019.05.023.

786 [82] S. Zhang,, Q. Wang,, P. Puthiaraj,, W.S. Ahn, Journal of CO2 Utilization  
787 34(June) (2019) 395–403. 10.1016/j.jcou.2019.07.035.

788 [83] F. Nakibuule,, S.A. Nyanzi,, I. Oshchapovsky,, O.F. Wendt,, E. Tebandeke,  
789 BMC Chemistry 14 (2020) 1–14. 10.1186/s13065-020-00713-2.

790 [84] Y. Kuwahara,, H. Yamashita, Biochemical Pharmacology 1 (2013) 50–9.  
791 10.1016/j.jcou.2013.03.001.

792 [85] S. Verma,, R.I. Kureshy,, T. Roy,, M. Kumar,, A. Das,, N.H. Khan,, S.H.R.  
793 Abdi,, H.C. Bajaj, Catalysis Communications 61 (2015) 78–82.  
794 10.1016/j.catcom.2014.12.013.

795 [86] Y. Kuwahara,, K. Tsuji,, T. Ohmichi,, T. Kamegawa, ChemSusChem 5  
796 (2012) 1523–32. 10.1002/cssc.201100814.

797 [87] S. Fujita,, B.M. Bhanage,, Y. Ikushima,, M. Shirai,, K. Torii, Catalysis  
798 Letters 79(April) (2002) 95–8. 1011-372X/02/0400-0095/0.

799